2020-08-03

Discovery of a Novel Regulatory Mechanism of TNK1 by 14-3-3 and Its Ubiquitin Association Domain Provides a Potential Therapeutic Targeting Opportunity in Cancer

Tsz Yin Chan
Brigham Young University

Discovery of a Novel Regulatory Mechanism of TNK1 by 14-3-3 and Its Ubiquitin Association Domain Provides a Potential Therapeutic Targeting Opportunity in Cancer

Tsz Yin Chan

A dissertation submitted to the faculty of
Brigham Young University
in partial fulfillment of the requirements for the degree of

Doctor of Philosophy

Joshua L. Andersen, Chair
Kenneth A. Christensen
Barry M. Willardson
Richard K. Watt

Department of Chemistry and Biochemistry

Brigham Young University

ABSTRACT

Discovery of a Novel Regulatory Mechanism of TNK1 by 14-3-3 and Its Ubiquitin Association Domain Provides a Potential Therapeutic Targeting Opportunity in Cancer

Tsz Yin Chan
Department of Chemistry and Biochemistry BYU
Doctor of Philosophy

While a relatively limited number of known oncogenes underlie a large percentage of cancers, a variety of new genes have emerged as low-frequency cancer drivers. Each of these new oncogenes represents a frontier for targeted therapy. However, the discovery of low-frequency targetable oncogenic drivers is challenging. This study focuses on the poorly understood Tyrosine kinase non-receptor-1 (TNK1), which has been reported to have both oncogenic and tumor suppressive functions. TNK1 has been identified to promote cancer cells survival and promote chemoresistance in multiple independent studies. On the other hand, whole-body constitutive deletion of TNK1 in mice caused an increase in spontaneous carcinomas and lymphomas. All in all, with no known regulatory mechanism and substrates of TNK1, the precise biological role of TNK1 is still unclear.

To understand how TNK1 is regulated, we employed a proteomic approach to identify TNK1 interactors. We found out that TNK1 interacts with the phospho-binding protein 14-3-3 and this interaction is mediated by a cluster of MARK-mediated phosphorylations within the proline-rich domain. 14-3-3 binding retains TNK1 in the cytosol and maintains TNK1 in an inactive state. Release of TNK1 from 14-3-3 binding drives TNK1 to a heavy membrane fraction, where it becomes highly active. One unique feature of TNK1 is an ubiquitin association domain (UBA) on its C-terminus. Our data suggest that the UBA domain of TNK1 binds to poly-ubiquitin chains in nondiscriminatory manner. Remarkably, point mutations within the UBA that disrupt ubiquitin binding abolish TNK1 activation and oncogenic signaling, suggesting a unique UBA-centric mechanism of tyrosine kinase regulation. Finally, we used a structure-guided approach to identify a small molecule inhibiting TNK1 with high potency and selectivity. This compound, TP-5801, inhibits TNK1 dependent STAT3 phosphorylation. TP-5801 also prolongs the survival of mice injected via tail vein with TNK1-driven Ba/F3 cells and reduces tumor burden in a subcutaneous xenograft model. In conclusion, our data reveal a mechanism of TNK1 regulation that controls its oncogenic tyrosine kinase activity and a potential strategy for TNK1 inhibition.

Keywords: TNK1, tyrosine kinase, kinase regulation, 14-3-3, ubiquitin association domain (UBA), STAT3, inhibitor

ACKNOWLEDGEMENTS

I would like to express my sincere gratitude to the following, who have helped towards this dissertation and helped me make it through my doctoral degree.

Thank you to my advisor, Dr. Joshua L. Andersen, for providing guidance, ideas and encouragement throughout this project, especially when the project did not seem to go anywhere and negative data came one after another. I also would like to thank my committee members, Dr. Barry M. Willardson, Kenneth A. Christensen and Richard K. Watt, for their input to the project. I greatly appreciate the funding that made this project possible. Funding was provided by Fritz B. Burns foundation, American Society Research Scholar Grant (133550-RSG-19-006-01-CCG) and National Cancer Institute/National Institutes of Health grant (2R15CA202618-02). I am also thankful for the Simmons Center for Cancer Research, the BYU College of Physical and Mathematical Sciences and the Roland K. Robins fellowship. I am also grateful to anyone who has worked on the TNK1 project, including professors, collaborators and lab members. Special thanks to Chrissy M. Egbert and Logan J. Larsen for working closely with me to push the project forward and towards publication.

Last but not least, a special gratitude is expressed towards my husband, Jeremy Tsang. He literally has walked along with me in the journey of getting a doctoral degree. Thank you for his love, encouragement, physical and mental support, especially after our daughter Cora was born. I also thank the Chan family and the Tsang family for supporting me to obtain the highest education possible.

TABLE OF CONTENTS

LIST OF TABLES AND FIGURES

1. Introduction

Tyrosine kinases act as mediators of signal transduction pathways and regulate a wide array of critical cellular processes such as cell survival, cell division and differentiation, apoptosis, gene expression and migration. In healthy cells, the activities of tyrosine kinases are tightly regulated to prevent unwanted survival or growth signaling. In cancer, these mechanisms of tyrosine kinase control are often overridden via mutation, gene amplification or rearrangement, resulting in aggressive cancer phenotypes. Indeed, tyrosine kinases have been implicated in many forms of cancer, including leukemia, lung cancer, breast cancer, colorectal cancer and pancreatic cancer. In recent years, tyrosine kinases have been recognized as high priority targets for anti-cancer treatments. Examples of clinically approved tyrosine kinase inhibitors include imatinib, dasatinib targeting BCR-Abl and gefitinib, erlotinib targeting EGFR.

With cancer sequencing projects and computational tools, many cancer driving proteins and mutations have been identified. However, these statistical methods often only capture the high frequency cancer drivers. While many of these frequent cancer drivers have been identified and are being exploited for therapeutic purposes, low frequency drivers are easily missed. Discovering low frequency driver genes is challenging yet important, as each of these new oncogenes represent a frontier for targeted therapy. Recent examples include NTRK fusions (e.g., 0.5-4% of colorectal cancer), ROS1 (1-2% of Non-small-cell lung carcinoma) and ALK (~4% of Non-small-cell lung carcinoma) all of which have therapeutics currently in the clinic[1-3].

There are two classes of tyrosine kinases: receptor tyrosine kinases (RTKs) and non-receptor tyrosine kinases (NRTKs). While RTKs function as cell surface receptors, NRTKs are cytosolic kinases that mediate the extracellular signals from receptors to intracellular effectors. Among NRTKs, there are several well-known oncogenes, such as SRC, JAK and ABL. Other than

these established oncogenic NRTKs, there are also potentially oncogenic NRTKs that remain uncharacterized as possible therapeutic targets. Our study focuses on one poorly characterized NRTK called Tyrosine Kinase Nonreceptor-1 (TNK1).

1.1. TNK1 is a member of the ACK subfamily of NRTK

NRTKs are categorized into different subfamilies based on their sequence and structure similarities. TNK1 is a member of the ACK subfamily of NRTKs, which includes only two human kinases, TNK1 and ACK1 (also known as TNK2). Other members include ACK2, DACK, DRP2 and Kos1. Specifically, ACK2 is a C-terminally truncated form of ACK1 identified in bovine brain. DACK and DRP2 are the Drosophila homologs of ACK1 with difference in domain structure. Kos1 is the murine homolog of TNK1.

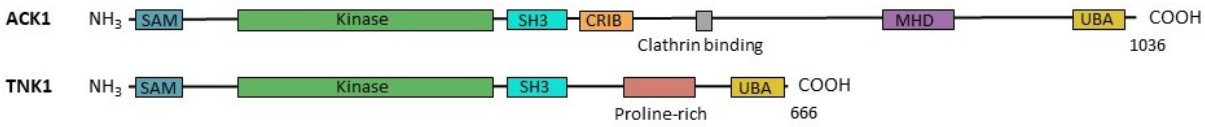

Figure 1-1 Domain structure of ACK1 and TNK1.

1.1.1. *Domain structure of the ACK family kinases*

TNK1 and ACK1 have a unique domain arrangement, highlighted by an N-terminal sterile alpha motif (SAM) domain, an SH3 domain immediately downstream of the kinase domain (both lack an SH2 domain), and a C-terminal ubiquitin association (UBA) domain (described in more detail below). In fact, TNK1 and ACK1 are the only two NRTKs with the SH3 domain C-terminal to the kinase domain. With such unique domain arrangement, the regulation of TNK1 and ACK1 are likely different from other NRTKs.

Domain	Function
SAM	Dimerization; membrane association[4]
SH3	Involved in autoinhibition[5, 6]
Cdc42/Rac-interacting domain	Binding to Cdc42[7, 8]
Clathrin-binding domain	Clathrin-mediated endocytosis [9, 10]
Mig6 homology domain	Involved in autoinhibition [5]

Table 1-1 Domains on ACK1 and their functions.

ACK1 is the more studied member of the ACK family and it possesses a large stretch of regulatory domains between its SH3 domain and UBA domain, including a Cdc42/Rac-interacting (CRIB) domain, a clathrin-binding domain and a Mig6 homology domain (MHD) (Figure 1-1). Intramolecular interactions between different domains of ACK1 contribute to its regulation. First, the SH3 domain of ACK1 appears to bind a proline-rich sequence at the C-terminal of MHD[5]. Such interaction is believed to position the MHD, allowing the inhibitory interaction with the kinase domain. Notably, activating mutations within the kinase domain (E346K) and SH3 domain (M409I) were reported in ovarian and stomach cancer respectively[11]. These mutations promote ACK1 activation by destabilizing the intramolecular interactions and thus release ACK1 from the autoinhibitory state. On the other hand, the role of the CRIB domain in regulating ACK1 activation is uncertain due to inconsistent results from independent studies[7, 8].

In contrast to ACK1, TNK1 does not possess these regulatory domains, which suggests regulatory difference between TNK1 and ACK1(Figure 1-1). TNK1 possesses a proline-rich domain between its SH3 domain and UBA domain, by which it interacts with phospholipase C-γ1[12]. This suggests that TNK1 might play a role in phospholipid-mediated signaling pathway. However, there is currently no known mechanism of TNK1 regulation nor established substrates.

In fact, TNK1 has been described to be constitutively active upon expression[12, 13]. Additional study is needed to understand the regulation and the biological role of TNK1.

1.1.2. *ACK kinases signaling and their role in cancer*

ACK1 has been reported to be activated by various ligands, including EGF, PDGF, heregulin and insulin[7]. This suggested that ACK1 is activated downstream of RTKs and acts as a cytosolic signal transducer to activate effector proteins. Upon EGF stimulation, ACK1 is activated and directly drives EGFR internalization and degradation/recycling[14, 15]. Being a regulator of EGFR trafficking, ACK1 indirectly regulates EGF-mediated pro-survival signaling. ACK1 is activated downstream of PDGFR as well. Upon PDGF stimulation, PDGFR directly phosphorylates ACK1 at Y635 to activate ACK1[16]. Sequential activation of ACK1 leads to AKT activation, nuclear translocation of β-catenin and cell cycle progression[16]. ACK1 has also been reported to regulate cell adhesion and cell migration. Upon binding to Cdc42, ACK1 directly phosphorylates p130Cas to promote cytoskeletal rearrangements and cell migration[17]. In addition, ACK1 has been reported to phosphorylate Histone H4 and promote androgen receptor expression[18]. ACK1 has also be shown to directly bind and phosphorylate androgen receptor to promote prostate cancer progression without androgen stimulation[19]. Indeed, ACK1 has been implicated as a proto-oncogene in prostate cancer, as well as leukemia, ovarian and breast cancer[18, 20-25]. Thus, ACK1 is a promising therapeutic target for cancer[26].

In contrast to ACK1, our knowledge on TNK1 is very limited. TNK1 was first cloned from umbilical cord blood hematopoietic stem/progenitor cells[27]. TNK1 is expressed in fetal tissues, but in adult tissues, it was described as limited to the prostate, testis, ovaries, colon and small intestine, with no detectable TNK1 in adult heart, brain, lung or other tissues[27, 28]. TNK1 high expression in fetal tissues suggest that TNK1 has an important role in embryonic development. TNK1 expression

has also been reported in various cancer cell lines, including leukemia, prostate cancer and ovarian carcinoma cells[28].

TNK1 had been identified in genome wide screens for sensitizers to gemcitabine in pancreatic cancer and Bortezomib in myeloma[29, 30]. In addition, in a retroviral insertion mutagenesis screen in Ba/F3 cells, TNK1 was identified as a moderately oncogenic kinase [31]. Furthermore, a hyperactive truncated form of TNK1 was identified in a patient-derived Hodgkin Lymphoma cell line as a result of paracentric inversion. This hyperactive form of TNK1 is the mediator of cell growth and survival of the lymphoma cell line [32]. While these studies suggest TNK1 to be an oncogenic NRTK, whole-body constitutive deletion of TNK1 in mice caused an increase in spontaneous carcinomas and lymphomas, primarily detectable within the gastrointestinal tract [33]—raising the question of whether TNK1 may also act as a tumor suppressor. Additional studies report that TNK1 regulates IFN signaling by potentiating STAT1 phosphorylation[34]. TNK1 is also reported as a negative regulator of NF-kB and Ras-Raf-MAPK pathway[12, 35, 36].

1.2. UBA domain

One unique feature of the ACK subfamily of NRTK is that they possess a the UBA domain[6]. UBA domain is a member of the alpha-helical family of the ubiquitin binding domains(UBDs). Other UBDs include ZnF (zinc finger), PH (pleckstrin-homology), Ubc-related (Ubiquitin-conjugating-related), SH3 and WD40 beta-propellers[37, 38]. There is no general ubiquitin binding consensus motif identified among all the UBDs. Within the alpha-helical family of UBDs, single alpha-helix and multiple alpha-helices can also define an alpha-helical UBD, and UBA

domains belong to the latter[38]. UBA domains are composed of three tightly packed □□helixes with a hydrophobic surface patch to mediate non-covalent interactions with mono- or poly-ubiquitin[38, 39]. UBA domains can be sorted into four classes based on their preference towards poly-ubiquitin linkages. Class 1 UBA preferably interacts with K48-linked poly-ubiquitin, class 2 UBA with K63-linked poly-ubiquitin and class 4 UBA domains bind poly-ubiquitin chains in a nondiscriminatory manner. On the other hand, class 3 UBA does not detectably bind ubiquitin[39].

UBA domains are often found in enzymes involved in proteasomal degradation, autophagy and DNA excision-repair pathways[39, 40]. Examples include the E3 ubiquitin ligase Cbl and the autophagy receptors p62/SQSTM1 and NBR1. The presence of a UBA domain on a kinase is unusual. Indeed, ACK kinases are the only tyrosine kinases with putative UBA domains. Among serine/threonine kinases, members of the AMPK family are the only kinases known to possess a UBA domain. However, these UBA domains show no appreciable affinity for ubiquitin. Instead, they form intramolecular interaction with the kinase domain to stabilize protein structure and regulate kinase activity[41-44]. For ACK kinases, the nature of their UBA domain—whether it interacts with ubiquitin and/or plays a role in kinase regulation— is still unclear. A study has shown that a somatic mutation in the UBA domain of ACK1 (S985N), initially identified in renal carcinoma cells, led to increased protein stability and increased cancer cell proliferation and migration[45]. However, there is no explanation for the effect of the mutation nor a clear mechanism of the function of the ACK1 UBA domain. Notably, ACK1 has been reported to directly interact with the autophagy receptor p62/SQSTM1 via its UBA domain and ACK1 was found to be localized on pre-autophagosome[14]. However, it is unclear whether ACK1 is a merely a substrate for degradation or plays a role in autophagy.

1.3. TNK1 interacts with the phospho-binding protein 14-3-3

Our preliminary data suggest that TNK1 interacts with the phospho-binding proteins 14-3-3s. The human 14-3-3 family includes seven different isoforms (β, γ, ε, η, σ, τ, and ζ). Although each isoform is expressed by a different gene, they are structurally similar[46]. Each isoform is consisted of nine α-helices that form an amphipathic groove. Within the grove, positively charged lysine and arginine residues (K49, K120, R56 and R127) are essential for 14-3-3 to interact with the phosphate of the binding partner[46, 47]. Acetylated modification of the lysine residues within or around the binding pocket may control 14-3-3 binding. 14-3-3 proteins function as homo- or hetero-dimers to interact with Ser/Thr-phosphorylated proteins with a general consenus sequence RXX[pS/T]XP[48]. For example, 14-3-3 binds to phosphorylated Bad at S75 and S99 (human numbering) with motif sequence of RHS[pS]YP and RSR[pS]AP respectively[49]. However, there are 14-3-3 binding sites that deviate from the consenus sequence as well[46, 48]. For example, transcription factor FOXO3 has a 14-3-3 binding of RAV[pS]MD[50]; Big mitogen-activated kinase 1 (BMK1/ERK5) has a 14-3-3 binding motif of LLK[pS]LR[51]. Both of these 14-3-3 binding motifs lack an arginine or a proline in the -3 and +2 positions.

14-3-3s possess no intrinsic enzymatic activity, but rather exert their effect through direct interaction with the phosphorylated binding partner. This effect can vary from inhibition or activation of catalytic activity, sequestration (e.g., out of the nucleus) and even scaffolding of protein-protein interactions[46]. 14-3-3s interact with a large network of phosphorylated proteins and essentially regulate all major signal transduction pathways. Since 14-3-3 isoforms share similar structure, the 14-3-3 isoforms overlap in their binding partners in many cases. Nevertheless, in some cases, there are also distinctive interactors and isoform-specific functions. Many proto-oncogenes and tumor suppressor proteins are regulated by 14-3-3s. For example, 14-3-3σ is known

to interacts with p53 to stabilize p53 for suppressing tumor growth[52]. 14-3-3σ expression has also been found to be reduced or lost in many human cancers, including breast, head and neck, liver and prostate cancers[53-56]. Therefore, 14-3-3σ has been generally considered a tumor suppressor among the 14-3-3 isoforms. (Yet, 14-3-3σ has also been shown to be overexpressed in multiple cancers where it has been shown to promote cell survival and cancer invasiveness[57, 58].) On the other hand, 14-3-3ζ is considered as an oncogene.14-3-3ζ is known to inhibit the pro-apoptotic protein Bad and also sequester Forkhead transcription factor in the cytoplasm, preventing the transcription of pro-apoptotic proteins[49, 50]. Overexpression of 14-3-3ζ correlates with cancer progression and chemoresistance[59-62].

14-3-3s are well-known regulators of kinases. For example, the kinase BRAF is locked into an inactive confirmation by 14-3-3 binding to pS365 and pS729 of the BRAF dimer, whereas rearrangement of 14-3-3 onto adjacent pS729 residues, spanning the BRAF dimer, locks the kinase into an active confirmation [63, 64]. Because 14-3-3 binding is dictated by phosphorylation, 14-3-3 interactions are inherently dynamic and responsive to changes in upstream kinase signaling. In this way, 14-3-3 acts as a central hub to orchestrate a variety of dynamic signaling events. Our preliminary data suggest that 14-3-3s bind to TNK1. However, at this point, the exact mechanism of how 14-3-3 is regulating TNK1 is still unknown.

2. A MARK- and 14-3-3-mediated mechanism restrains a ubiquitin-dependent mode of TNK1 activation that can be inhibited to suppress tumor growth *in vivo*

*This chapter is currently under review with minor variations from this version:

Chan, TY., Egbert, C.M., Maxson, J.E., Larsen, L.J., Kohler, K., Balasooriya, E.R., Pennington, K.L., Tsang, TM., Frey, M., Geng, H., Müschen, M., Free, S., Mercenne, G., Banks, C.J., Valdoz, J., Whatcott, C.J., Foulks, J.M., Siddiqui, A., Bearss, D.B., O'Hare, T., Huang, D.CS., Christensen, K.A., Moody, J., Warner, S.L., Tyner, J.W., Andersen, J.L., *A MARK- and 14-3-3-mediated mechanism restrains a ubiquitin-dependent mode of TNK1 activation that can be inhibited to suppress tumor growth in vivo.*

2.1. Abstract

TNK1 is a poorly understood member of the ACK family of non-receptor tyrosine kinases. In this study, we identify TNK1 as a mediator of cell survival in a subset of primary specimens from lymphoid malignancy patients. We discover a MARK-mediated phosphorylation on TNK1 at S502 that promotes an interaction between TNK1 and 14-3-3, which sequesters TNK1 and inhibits its kinase activity. Conversely, the release of TNK1 from 14-3-3 allows TNK1 to cluster in membrane-associated cytosolic puncta and become active. In this active state, TNK1 potently induces growth factor-independent proliferation of lymphoid cells in cell culture and mouse models. One feature of TNK1 is a ubiquitin-association domain (UBA) on its C-terminus, which sits adjacent to the 14-3-3 binding site. Here, we characterize the TNK1 UBA and find that it has high affinity for a variety of poly-ubiquitin linkages. Remarkably, point mutations within the UBA that disrupt ubiquitin binding, also inhibit TNK1 activation and oncogenic signaling. These data support a mechanism in which TNK1 toggles between 14-3-3-bound (inactive) and ubiquitin-bound (active) states, thereby revealing a new paradigm of UBA involvement in kinase regulation. Finally, we use a structure-guided approach to identify a small molecule TNK1 inhibitor with high potency and selectivity. This compound, TP-5801, shows nanomolar potency against TNK1-

driven cells, prolongs the survival of mice injected with these cells via tail vein, and reduces disease burden in mice with subcutaneous xenograft tumors. Together, our data reveal a novel 14-3-3- and UBA-mediated mechanism of tyrosine kinase regulation and identify a lead compound for further development of a TNK1 inhibitor.

2.2. Introduction

Non-receptor tyrosine kinases (NRTKs) comprise several subfamilies of intracellular tyrosine-directed kinases. Although these kinases differ to varying degrees in structure, many exploit the same pathways to regulate cancer-relevant processes, including apoptosis, proliferation and motility. The NRTK superfamily includes established oncogenes, such as SRC, ABL, JAK and SYK-ZAP-70, many of which have been exploited for targeted therapy[65]. Beyond these established oncogenic NRTKs is a subset of NRTKs that remain poorly understood and relatively untapped as potential therapeutic targets.

Non-receptor tyrosine kinase (also known as Thirty-eight-negative kinase-1 or TNK1) is a poorly understood kinase in the ACK family of NRTKs. TNK1 emerged as a top hit in genome wide screens for sensitizers to chemotherapy in pancreatic cancer and myeloma[29, 30]. In addition, a retroviral insertion screen in Ba/F3 cells identified TNK1 as having moderate oncogenic activity[31]. Furthermore, a truncated, constitutively active form of TNK1 was identified in a Hodgkin lymphoma (HL) cell line, which was dependent on TNK1 for growth and survival[32]. While these studies cast TNK1 as an oncogenic NRTK, whole-body constitutive deletion of TNK1 in mice caused an increase in spontaneous carcinomas and lymphomas, primarily detectable within the gastrointestinal tract[33] —raising the question of whether TNK1 may also act as a tumor

suppressor. However, there is currently no known mechanism of TNK1 regulation nor established TNK1 substrates, and its biological role remains unclear.

Here, we identify TNK1 as a mediator of cell survival in primary lymphoid malignancies and uncover a mechanism of TNK1 regulation. We discover that a MARK-mediated interaction between 14-3-3 and TNK1 restrains TNK1 localization and activity. This mechanism also involves an unusual interplay between the TNK1 UBA, ubiquitin binding and TNK1 kinase activity, demonstrating a novel example of kinase modulation via direct, non-covalent interaction with ubiquitin. Importantly, disruption of 14-3-3 binding to TNK1 dramatically enhances TNK1-driven proliferation in a UBA-dependent manner in cell culture and mouse models. Lastly, we develop a selective and potent small molecule inhibitor that blocks TNK1-mediated cell proliferation *in vivo*. Together, our data demonstrate the first mechanism of TNK1 regulation, a new paradigm of UBA-ubiquitin interaction in tyrosine kinase activation, and a lead compound against TNK1.

2.3. Methods

2.3.1. *Antibodies*

The following antibodies were purchased from Cell Signaling Technology: DYKDDDDK tag mouse mAb (8146S), HA-tag mouse (2367S), Phospho Tyrosine (pTyr 1000) Rabbit mAb (8954S), Ubiquitin Antibody Rabbit (3933S), Ubiquitin Mouse mAb (3936S), MARK3 (9311S), GST Mouse mAb (2624S), STAT1 (14994), Phospho-Stat3 (Tyr705) Mouse mAb (4113), Stat3 rabbit mAb (12640), Phospho-Stat5 (Tyr694) (4322), Stat5 (25656) GFP mouse mAb (2955S) and phospho-PLCγ1 (Tyr783). Monoclonal ANTI-FLAG M2 antibody (F1804) was purchased from Sigma-Aldrich. 14-3-3 Pan Polyclonal Antibody (510700) was purchased from Thermo Fisher Scientific. VU-1 ubiquitin antibodies (VU101) was purchased from LifeSensors. MARK1 (21552-

1-AP) and MARK2 (15492-1-AP) antibodies were purchased from Proteintech Group. MARK4 antibody (MBS8208929) was purchased from MyBioSource.

2.3.2. *Reagents and inhibitors*

Lipofectamine RNAiMAX (13778150), Pierce Protease Inhibitor Tablets (EDTA Free) (88266), Pierce Phosphatase Inhibitor Mini Tablets (A32957), B PER Bacterial Protein Extraction Reagent (78248), lysozyme (89833), DNaseI (90083), SEABLOCK Blocking Buffer (37527), Life Technologies Prolong Diamond Antifade (P36961) and Pierce High Capacity Streptavidin Agarose (20357) were purchased from Thermo Fisher Scientific. MARK1, MARK2, MARK3, MARK4 ON-TARGETplus siRNA (L-004259-00-0010, L-004260-00-0010, L-003517-00-0010, L-005345-00-0010) were purchased from Dharmacon. Transporter 5 (26008-50) was purchased from Polysciences and Viafect Transfection Reagent (E4981) was purchased from Promega. Recombinant Mouse IL-3 Protein (403-ML-010) was purchased from R&D systems. Biosensor - Anti-GST (GST) Tray (18-5096) was purchased from ForteBio. AQUApure Linear Tetra-Ub Chains (M1-link) CF (UC-710B-025), AQUApure Tetra-Ub Chains (K6-linked) Protein, CF (UC-15-025), AQUApure Tetra-Ub Chains (K11-linked) Protein, CF (UC-45-025), AQUApure Tetra-Ub Chains (K29-linked) Protein, CF (UC-83-025), AQUApure Tetra-Ub Chains (K33-linked) Protein, CF (UC-103-025), AQUApure Tetra-Ub Chains (K48-linked), CF (UC-210B-025), AQUApure Tetra-Ub Chains (K63-linked), CF (UC-310B-025), Ubiquitin (U-100H), Poly-Ubiquitin/Ub2-Ub7 WT Chains (K48-linked) (UC-230) and Poly-Ubiquitin/Ub2-Ub7 WT Chains (K63-linked) (UC-330) were purchased from Boston Biochem. Biotin (B4639-1G), Polybrene Transfection reagent (TR-1003-G) and ANTI-FLAG M2 Affinity Gel (A2220) were purchased from Sigma-Aldrich. Phosphoblocker Blocking Reagent (AKR-103) was

purchased from Cell Biolabs. Luciferase Assay Systems (E1500, E4030) were purchased from Promega. Human TNK1 ORF clone in pcDNA3.1 (OHu15330C) and Anti-DYKDDDDK G1 Affinity Resin (L00432) were purchased from GenScript.

STO-609 (acetate) (15325), KN-62 (13318), BMS 345541 (trifluoroacetate salt) (16667), LJI308 (19924) and Niclosamide (10649) were purchased from Cayman Chemical Company. Asciminib (S8555) was purchased from Selleck Chemicals. MRT67307 (5.06306.0001) was purchased from EMD Millipore Corporation. KN-93, ≥98% (hplc) (K1385) was purchased from Sigma-Aldrich. KN-93, Water-Soluble (422711) were purchased from Millipore Sigma. Hygromycin B (10687010) and Puromucin Dihydrochloride (A1113803) were purchased from Thermo Fisher Scientific.

2.3.3. *Maintenance of cell lines*

HEK293T, HEK293A and A549 were purchased from ATCC and cultured in DMEM supplemented with 10% FBS. Ba/F3 and FDCP1 cells were purchased from DSMZ-German Collection of Microorganisms and Cell Cultures and were cultured in RPMI supplemented with 10% FBS, 1 mM sodium pyruvate, 10 mM HEPES, 1% Pen/Strep and 1 ng/mL mIL-3. HEK-293T Lenti-X were purchased from Takara Bio and cultured in DMEM supplemented with 10% FBS. L540 were purchased from DSMZ-German Collection of Microorganisms and Cell Cultures and were cultured in RPMI supplemented with 20% FBS. All cells are incubated at 37ºC with 5% CO_2.

2.3.4. *Viral transduction*

The retroviral firefly luciferase reporter plasmid, pMIG-BCR-ABL, packaging and envelope plasmids were generous gifts from Dr. Michael Deininger's group. The retroviral pMSCV-IRES-GFP II (pMIG II) was a gift from Dario Vignali (Addgene plasmid # 52107). pLenti-puro was a gift from Ie-Ming Shih (Addgene plasmid # 39481). To generate retrovirus, retroviral transfer and envelope/packaging plasmid were transfected into HEK-293T Lenti-X cells (Takara Bio) with Transporter 5 transfection reagent (Polysciences) according to manufacturer's protocol. 48-72 hours post transfection, retrovirus in the media were collected and centrifuged at 500xg for 5 min to clear out cell debris. To generate lentivirus, viral transfer plasmid (pLenti-puro or pMIG) was transfected together with the packaging (pCMV-Δ8.2Δvpr) and envelop plasmid (pVSVG) into HEK-293T Lenti-X cells with Transporter 5 transfection reagent (Polysciences) according to manufacturer's protocol. 48-72 hours post transfection, lentiviral supernatant was collected and centrifuged at 500xg for 5 min to clear out cell debris.

2.3.5. *Generation of cell lines*

To generate the Ba/F3 luciferase cell line, Ba/F3 cells were spinfected with firefly luciferase reporter retrovirus with 10 ug/mL polybrene for 2 hours at 800xg at room temperature. Transduced cells were incubated with the retrovirus for an additional 4 hours before transferring to fresh complete growth medium. 48 hours after spinfection, transduced cells were selected with 1 mg/mL hygromycin for 10 days. The hygromycin-resistant Ba/F3 luciferase cell line was sorted in the presence of propidium iodide stain to one-cell-per-well into 96 well plate with BD FACSAria Fusion flow cytometer (BD). The sorted hygromycin-resistant Ba/F3 luciferase cell lines were tested in a luciferase reporter assay (Promega) approximately two weeks later.

To generate the HA-14-3-3 HEK293T cell line, HEK293T cells were stably transduced with HA-14-3-3ζ-expressing lentivirus. 48 hours post-transduction, puromycin was added to the cells at final concentration of 3 ug/mL for 48 hours to select the transduced cells. Stable expression of 14-3-3ζ was validated by immunoblot.

To generate the FLAG-TNK1 A549 cell line, A549 cells were stably transduced with FLAG-TNK1-expressing lentivirus. 48-hour post-transduction, cells are sorted for GFP-positive with BD FACSAria Fusion flow cytometer (BD). Stable expression of FLAG-TNK1 was validated by immunoblot.

2.3.6. *Mutagenesis and cell transfection*

FLAG-TNK1 expression plasmid was purchased from GenScript. All mutagenesis was performed using Q5 Site-Directed Mutagenesis Kit (NEB), following the manufacturer's protocol. Cells were plated one day before transfection to obtain 40-50% cell confluency at the day of transfection. Transfection complex was prepared at 1:4 DNA/transporter 5 ratio in DMEM and incubated at room temperature for 20 minutes. After DNA-transporter 5 complexes were added to the cells, cells were returned to the incubator. Media were replaced after 6 -8 hours.

2.3.7. *Immunoprecipitation and Immunoblot*

For TNK1 or 14-3-3 immunoprecipitation, transfected, transduced or stably expressing HEK293T or A549 cells were washed and harvested in ice-cold PBS. Cell pellets were lysed in either co-IP lysis buffer (10mM HEPES KOH pH 7.5, 150mM KCl, 0.01% IGEPAL)

supplemented with protease and phosphatase inhibitors and rotated at 4ºC for 10 mins. Lysates were then homogenized by passaging through a 25G needle and centrifuged at 21000xg for 10 mins to clarify. Clarified lysate were collected for immunoprecipitation and/or western blot. For FLAG or HA pulldown, lysates were incubated with anti-DYKDDDDK G1 Affinity Resin (GenScript) or Anti-HA−Agarose (Millipore Sigma) for 1 hour at 4ºC with rotation. The resins were washed with PBS three times. The coimmunoprecipitated proteins were eluted with SDS sample buffer by boiling at 96ºC for 5 mins. Lysate were resolved by SDS-PAGE and transferred to nitrocellulose membrane using iBlot2 Western Blotting System. Membranes were blocked with either 5% non-fat dry milk in PBS, intercept blocking buffer (Li-cor), or 5% phosphoblocker (Cell Biolabs) in PBST for 1 hour at room temperature. Primary antibodies against proteins of interests were diluted 1:500 or 1:1000 in blocking buffer and incubated with blot overnight at 4ºC. Proteins were visualized and quantified using infrared fluorescent secondary antibodies (Li-cor) and Li-Cor Odyssey imaging system.

Transduced Ba/F3 cells were harvested and lysed in tris-triton lysis buffer (50mM Tris pH8.0, 150mM NaCl, 1% Triton X-100) supplemented with protease and phosphatase inhibitors (ThermoFisher Scientific). Lysates were incubated on ice and vortexed every 2 mins for 10 mins. Lysates were then centrifuged at 21000xg for 10 mins and the supernatants were transferred to new tubes. Lysates were then mixed with 5X SDS sample buffer and boiled at 96ºC for 5 mins. Western blotting was performed as described above.

2.3.8. *BioID*

MCS-BioID2-HA was a gift from Kyle Roux (Addgene plasmid # 74224). TNK1 cDNA sequence was cloned into MCS-BioID2-HA (addgene), so that the biotin ligase BirA is C-terminal to TNK1. TNK1-BirA-HA was transfected into HEK-293T cells as described above. 36 hours post-transfection, 50 nM of biotin was added to cells and the cells were returned to the incubator for 10 hours. Cells were washed with ice-cold PBS three times before harvesting and lysed with RIPA without SDS (1 M Tris pH 7.5, 10% sodium deoxycholate, 3 M NaCl, 10% Triton X 100) as described above. Clarified lysates were incubated with Streptavidin Agarose (Thermo Fisher Scientific) for 1 hour at 4ºC with rotation. The resins were washed 4 times with lysis buffer. Western blot was performed as described above.

2.3.9. *siRNA silencing*

Cells were seeded at 40% confluence and washed with PBS 2 times, and then Opti-MEM (ThermoFisher Scientific) was added to the cells. The siRNA complex was prepared by incubating Lipofectamine RNAiMAX (ThermoFisher Scientific) and siRNA for various targets at 100 nM final concentration for 20 minutes. The complex was then added to cells and incubated for 4 hours, after which FBS was added. After additional 8 hours of incubation, media was changed and transfection was performed as needed.

2.3.10. *RNAi screening of patient samples*

Detailed description of the RNAi assisted protein target identification (RAPID) can be found elsewhere[66, 67] . In short, peripheral blood, bone marrow aspirates or leukapheresis samples were obtained from cancer patients through informed consent via a protocol approved by the

Oregon Health & Science University Institutional Review Board. Peripheral blood mononuclear cells (PMBCs) were isolated through a Ficoll gradient and aliquoted into a 96-well plate containing 91 arrayed siRNA pools targeting the tyrosine kinome. After electroporation of siRNAs, cells were transferred to standard cell culture media, incubated 96 hours and assayed for viability by a tetrazolium-based MTS assay. Positive "hits" were scored for targets that reduced cell viability by at least two standard deviations below the mean of all siRNAs on a given sample run. RNAi silencing was confirmed by immunoblotting and qPCR. All hits were assessed by unsupervised hierarchical clustering for each patient sample. Data were analyzed in R.

2.3.11. *Heavy membrane fractionation*

Cells were scraped from plate and rinsed with cold PBS. Cells were pelleted and then resuspended in TEB buffer (300 mM Trehalose, 10 nM HEPES-KOH pH7.7, 80 mM KCL, 1 mM EDTA, 5 mM Succinate) with 0.025% digitonin. Samples were left on ice for 10 minutes, mixing every 2 minutes. The sample were centrifuged at 13000 rpm for 4 min to pellet the heavy membrane fraction, and the supernatant was collected as the cytosolic fraction. The pellet was then resuspended in RIPA buffer without SDS (1 M Tris pH 7.5, 10% sodium deoxycholate, 3M NaCl, 10% Triton X 100) and incubated on ice for 10 minutes. The samples were centrifuged for 3 min at 3000 rpm and the supernatant was collected as the heavy membrane fraction. Samples were mixed with SDS sample buffer, boiled, and loaded onto SDS-PAGE gels and subsequently western blotted.

2.3.12. *Expression/purification of UBA domain and Ubiquitin pull down assay*

cDNA fragments for the human TNK1 or TAB2 UBA domains were cloned into the pGEX-6P-1 vector with GST on the N-terminus of the UBA domain. GST-only and GST-UBA plasmids were transformed into BL21 E. coli. IPTG was added to induce expression for 3 hours at 37ºC after OD600 reached 0.5-0.7. Bacteria were then centrifuged and washed with ice-cold 0.9% NaCl solution once. Bacterial pellets were lysed with B-PER (Thermo Fisher Scientific) supplemented with DNase I, lysozyme, and protease Inhibitor, according to manufacturer's protocol. The cleared bacterial lysates were incubated with glutathione agarose resin (Goldbio) for 2 hours at 4ºC with rotation. The resins were washed with washing buffer (10mM HEPES pH7.5, 300mM NaCl, 1mM DTT) three times. Immobilized GST fusion proteins were incubated with 0.5µg of recombinant ubiquitin in ubiquitin pulldown buffer (150 mM NaCl, 50 mM Tris pH 7.5, 0.1% IGEPAL, 5 mM DTT, 0.25 mg/mL BSA) for 2 hours at 4ºC with rotation. Immobilized GST fusion proteins were washed four times with ubiquitin pulldown buffer. Proteins were eluted from the resins in SDS sample buffer with 5 mM DTT in 38ºC for 20 mins. Proteins were then resolved by SDS-PAGE as described above.

2.3.13. *Bio-layer interferometry (BLI)*

Pellets of BL21 E. Coli expressing either GST-TNK1-UBA or GST-TAB2-UBA were lysed with B-PER bacterial protein extraction reagent supplemented with DNaseI, lysozyme, and protease inhibitor according to the manufacture protocol. Assay buffer was 50 mM Tris, 150 mM NaCl, pH 7.2, 0.1% NP-40, 0.25 mg/mL BSA, with 5 mM DTT supplement added fresh upon each use. Assays were done using an Octet RED96 biolayer interferometer (ForteBio) and were performed at 30°C and 1000 rpm shaking. First, Anti-GST biosensors (ForteBio) were loaded with GST-TNK1-UBA lysate (8 sensors, 6 for tetra-ubiquitin binding, 2 for reference control) or GST-

TAB2-UBA lysates (4 sensors, 3 for tetra-ubiquitin binding, 1 for reference control) for 60 seconds. The loaded sensors were then equilibrated in assay buffer (360 sec) followed by an association step with a serial dilution. For TNK1-UBA, K48 tetra ubiquitin ranged from 25 nM to 0.8 nM; K63 ranged from 20 nM to 0.6 nM, for 60 seconds followed by dissociation in assay buffer for 300 seconds. K63 and K48 tetra-ubiquitin in TAB2-UBA assay ranged from 200 nM to 50 nM, with association for 5 or 60 seconds, respectively, followed by a 60 second dissociation. Data was processed and analyzed in the Octet Data Analysis 8.2 software. Processed data was fit to a 1:1 binding model to obtain kinetic and thermodynamic parameters. Residuals were examined to assess quality of fit and no systematic deviation was observed.

2.3.14. *IL-3 independent growth assays*

FDCP1, Ba/F3 or Ba/F3 stable luciferase-expressing cells were transduced as stated previously in cell line development. Two days after transduction, cell were sorted for the GFP positive population with BD FACSAria Fusion flow cytometer (BD). The positive population was seeded in 24 well plates 50,000 cells per well in media without IL3. These cells were imaged using Essen Bioscience IncuCyte ZOOM 10X objective every 4 hours for 10 days. Rate of transformation is determined by the time required to reach 20% cell confluency.

2.3.15. *Phospho-tyrosine proteomics*

An analysis of the phospho-tyrosine substrate network was performed on the IL-3-independent WT TNK1-, TNK1-AAA- and BCR-ABL-driven Ba/F3 cells. These cells were compared to control Ba/F3 cells that had been withdrawn from IL-3 for 24 hours to establish a

baseline level of global phospho-tyrosine. Quantitative phospho-tyrosine proteomics was performed by the Duke University School of Medicine Proteomics and Metabolomics Shared Resource. Briefly, $2x10^8$ Ba/F3 cells were collected and rinsed with ice-cold PBS. Cell pellets were flash-frozen and sent to the Duke Proteomics Core Facility (DPCF). After addition of urea, cell pellets were subjected to three rounds of probe sonication for 5 sec each with an energy setting of 30%. Samples were then centrifuged at 12,000xg at 4°C for 5 min. Protein concentrations were determined by Bradford assay. 10 mg of each sample were normalized with 8 M urea and then diluted to 1.6 M urea with 50 mM ammonium bicarbonate. All samples were then reduced for 45 min at 32°C with 10 mM dithiolthreitol and alkylated for 30 min at room temperature with 25 mM iodoacetamide. Trypsin was added to a 1:50 ratio (enzyme to total protein) and allowed to proceed for 18 hr at 32°C. Samples were then acidified with TFA and subjected to C18 SPE cleanup (Sep-Pak, 500 mg bed). Following elution, all samples were then lyophilized to dryness then resuspended in PBS. Samples were subjected to immunoaffinity purification and enriched for tyrosine phosphopeptides using PTMScan (Cell Signaling Technology), then lyophilized. At this point, the sample was subjected to simple TiOx enrichment after being spiked with a total of either 2.5 or 5 pmol of casein for internal standard quality control, then lyophilized again. Samples were resuspended in 12 µL 1%TFA/2% acetonitrile with 10 mM citrate containing 12.5 fmol/µL yeast alcohol dehydrogenase (ADH_YEAST). From each sample, 2 µL was removed to create a QC Pool sample which was run periodically throughout the acquisition period.

2.3.16. *TiO_2 phospho-proteomics*

HEK293T cells were transfected with either FLAG-TNK1 WT or FLAG-TNK1-ΔUBA with PEI. 48hours post transfection, cells were harvested and lysed as descried above. All buffers

were prepared with HPLC-grade-water. Clarified lysate were incubated with ANTI-FLAG® M2 Affinity Gel for 1hour in 4ºC. Resin were washed with cold PBS supplemented with protease and phosphatase inhibitors twice and then three times with Ambic solution (50mM ammonium bicarbonate in water). The proteins were eluted with elution buffer (0.25% rapigest SF in 50mM ammonium bicarbonate) and boiled for 3 mins. Samples were flash-freeze and sent to the Duke Proteomics Core Facility (DPCF) for further preparation. Samples were prepared for in-solution digestion, TiOx enrichment and LC-MS/MS Analysis as described above

2.3.17. *Quantitative LC-MS/MS Analysis*

Quantitative LC-MS/MS was performed on 4 µL of each Ba/F3 tyrosine phosphopeptide sample, using a nanoAcquity UPLC system (Waters Corp) coupled to a Thermo Orbitrap Fusion Lumos high resolution accurate mass tandem mass spectrometer (Thermo) via a nanoelectrospray ionization source. Briefly, the sample was first trapped on a Symmetry C18 20 mm × 180 µm trapping column (5 µl/min at 99.9/0.1 v/v water/acetonitrile), after which the analytical separation was performed using a 1.8 µm Acquity HSS T3 C18 75 µm × 250 mm column (Waters Corp.) with a 90-min linear gradient of 3 to 30% acetonitrile with 0.1% formic acid at a flow rate of 400 nanoliters/minute (nL/min) with a column temperature of 55ºC. Data collection on the Fusion Lumos mass spectrometer was performed in a data-dependent acquisition (DDA) mode of acquisition with a r=120,000 (@ m/z 200) full MS scan from m/z 375 – 1500 with a target AGC value of $2x10^5$ ions. MS/MS scans were acquired at Rapid scan rate (Ion Trap) with an AGC target of $5x10^3$ ions and a max injection time of 200 ms. The total cycle time for MS and MS/MS scans was 2 sec. A 20 sec dynamic exclusion was employed to increase depth of coverage. The SPQC pool containing an equal mixture of each sample was analyzed after every 4 samples throughout the entire sample set.

Next, data were imported into Proteome Discoverer 2.3 (Thermo Scientific Inc.) and all LC-MS/MS runs were aligned based on the accurate mass and retention time of detected ions ("features") which contained MS/MS spectra using Minora Feature Detector algorithm in Proteome Discoverer. Relative peptide abundance was calculated based on area-under-the-curve (AUC) of the selected ion chromatograms of the aligned features across all runs. Peptides were annotated at a maximum 1% peptide spectral match (PSM) false discovery rate.

The MS/MS data were searched against the SwissProt M. musculus database (downloaded in Apr 2018) and an equal number of reverse-sequence "decoys" for false discovery rate determination. Mascot Distiller and Mascot Server (v 2.5, Matrix Sciences) were utilized to produce fragment ion spectra and to perform the database searches. Database search parameters included fixed modification on Cys (carbamidomethyl) and variable modifications on Meth (oxidation); Asn/Gln (deamidation); Ser/Thr/Tyr (phosphorylation).

2.3.18. *TNK1 WT and ΔUBA Phospho-Proteomics*

HEK293T cells were transfected with either FLAG-TNK1 WT or FLAG-TNK1 ΔUBA with PEI. 48 hours post-transfection, cells were harvested and lysed as descried above. All buffers were prepared with HPLC-grade water. Clarified lysate were incubated with ANTI-FLAG M2 Affinity Gel (Simga Aldrich) for 1 hour at 4ºC. Resins were washed with cold PBS supplemented with protease and phosphatase inhibitors twice and then with Ambic solution (50 mM ammonium bicarbonate in water) three times. The proteins were eluted with elution buffer (0.25% rapigest SF in 50 mM ammonium bicarbonate) and boiled for 3 mins. Samples were flash-frozen and sent to the Duke Proteomics Core Facility (DPCF) for further preparation. Samples were prepared for in-solution digestion, TiOx enrichment and LC-MS/MS analysis as described above.

2.3.19. *Confocal*

pEGFP-N1-FLAG was a gift from Patrick Calsou (Addgene plasmid # 60360). TNK1 was cloned into pEGFP-N1-FLAG plasmid, so that the EGFP tag is C-terminal to TNK1. HEK293A cells were seeded on coverslips and transfected with appropriate constructs. The next day, cells were fixed with 4% PFA in PBS for 10 minutes and permeabilized with 0.1% Triton X-100 (in PBS). Cells were blocked using Seablock Blocking Buffer (ThermoFisher Scientific) at room temperature for 1 hour. Primary antibodies were added in diluted blocking buffer (10% Seablock Blocking Buffer in PBS with 0.1% Tween) overnight at 4°C. Coverslips were washed 3 times with PBS, and then incubated with Alexa Fluor-conjugated secondary antibodies at a 1:1000 dilution in Seablock Blocking Buffer for 1 hour at room temperature. DAPI was added for the last 5 minutes at a 1:100 dilution. Coverslips were then washed with PBST once followed by 2 washes with PBS. Coverslips were mounted on slides using ProLong Diamond Antifade Mountant (ThermoFisher Scientific) and cured for 24 hours before imaging. Imaging was performed using Leica TCS SP8 DMi8 confocal laser microscope using at 63X oil-immersion lens. After acquisition, images were processed using Huygens Deconvolution software and Leica 3D analysis software. Image channels were acquired sequentially using appropriate settings for DAPI, eGFP, and Alexa Fluor 663. Representative images are shown within figures. Quantification was performed by counting 50 cells per slide and condition visually for phenotype, designated as punctuate or diffuse. In all experiments, images shown within panels were all acquired using identical intensity and exposure time at room temperature.

2.3.20. *14-3-3ζ-TNK1 FRET Assay*

The FRET assay was performed as adapted from Du. et. al., 2013. Briefly, His-14-3-3ζ (12 nM final, R&D Systems); Cy5-TNK1, Cy5-p502-TNK1, or Cy5-p500/p502/p505-TNK1 (10 µM final, 5 µM final, and 1 µM final for each peptide; New England Peptide); Europium-anti-His antibody (0.75 nM final, PerkinElmer), and Bovine Serum Albumin (2 µg) were added to FRET buffer (20 mM Tris, pH 7.4, 0.1% Nonidet P40 and 50 mM NaCl; adapted from Du et. al. 2013) for a final volume of 30 µL per reaction. Negative control reactions were performed as half the reactions without 14-3-3ζ to determine background fluorescence transfer. For the positive control reactions, Cy5-p136-BAD (12.5 µM final, New England Peptide), a known 14-3-3ζ interacting partner, was added instead of TNK1. The assay was performed in a black, flat-bottom, 384-well plate (Corning), with reactions done in quadruplicate. The plate was covered and incubated for 2 hours at room temperature. Then, the fluorescence was measured using the PerkinElmer EnVision Multimode plate reader, excitation: 340 nm, emission: 615 nm and 665 nm. FRET ratios were determined by dividing the 615 nm fluorescence value by the 665 nm fluorescence value, and multiplying by 103. Peptide sequences were as follows:

Cy5-TNK1 Sequence: H2N-(C/Cy5Mal)RMKGISRSLESVLSLGP-amide;

Cy5-p502-TNK1 Sequence: H2N-(C/Cy5Mal)RMKGISR(pS)LESVLSLGP-amide;

Cy5-p500/p502/p505-TNK1 Sequence: H2N-(C/Cy5Mal)RMKGI(pS)R(pS)LE(pS)VLSLGP-amide;

Cy5-p136-BAD Sequence: H2N-(C/Cy5Mal)LSPFRGRSR(pS)APPNLWA-OH

2.3.21. *Development of TNK1 inhibitor – TP-5801*

The active site of the TNK1 homology model was built using an ALK crystal structure (PDB code 4MKC) as a template (ICM-Pro, Molsoft). TP-5801 was designed using computational chemistry techniques based on initial diaminopyrimidine "hit" compounds from an in-house library, which was screened in a biochemical assay against a truncated recombinant TNK1 (encompassing the kinase domain).

2.3.22. *Tumor progression study in mice*

$1x10^6$ Ba/F3 luc cells expressing vector (pMIG), WT TNK1, TNK1 mutants (as indicated), or BCR-ABL were injected into the tail vein of both male and female NOD/SCID mice (n=5 for each group). Mice were imaged in both prone and supine position using an IVIS Spectrum in vivo imaging system (Perkin Elmer). Bioluminescent signals were quantified using Living Image 4.3.1 (Caliper Life Sciences). Signals were analyzed by region of interest (ROI) analysis, which measured total body flux (photons/second) over time. Moribund animals were sacrificed as per IACUC guidelines. Survival data were analyzed using Kaplan-Meier method, and statistical significance was evaluated with a Log-rank test (GraphPad PRISM) comparing the survival time of each group.

2.3.23. *Drug study on tail vein-injected mice*

$1x10^6$ Ba/F3 luc cells expressing TNK1 AAA were injected into the tail vein of female NOD/SCID mice. (n=5 for each group). 3 days after injection, mice were treated once daily by oral gavage with vehicle (0.5% Methylcellulose (w/v), 0.5% Tween 80 (v/v), 99% H2O (v/v)) or TP5801 (10 mg/kg). Moribund animals were sacrificed as per IACUC guidelines. Survival data

were analyzed using Kaplan-Meier method, and statistical significance was evaluated with a Log-rank test (GraphPad PRISM) comparing the survival time of each group.

2.3.24. *Drug study on Sub-Q mice*

$1x10^6$ Ba/F3 luc cells expressing TNK1-AAA were implanted subcutaneously into the flank of NOD/SCID mice. Mice were randomized to treatment groups (n=10) when the average tumor volume reached approximately 100-200 mm3. Mice were treated once daily by oral gavage with vehicle (0.5% Methylcellulose (w/v), 0.5% Tween 80 (v/v), 99% H_2O (v/v)), or TP5801 (50 mg/kg) for up to 7 consecutive days. Bioluminescent signals were imaged, quantified, and analyzed as mentioned above. Mice were sacrificed and tumor samples were collected. Tumor samples were weighed. Some tumor samples were flash frozen and some were paraffin embedded.

2.3.25. *In vitro kinase screen*

The abilities of 245 individual Ser/Thr kinases to phosphorylate a TNK1 peptide that includes S502 were evaluated using a radiometric KinaseFinder assay (ProQinase GmbH). A biotinylated peptide (Biotin-RMKGISRSLESVL-OH; New England Peptide) was reconstituted in 50 nM HEPES pH 7.5 at 200 µM stock solution. Reaction buffer (60 mM HEPES-NaOH pH 7.5, 3 mM $MgCl_2$, 3 mM $MnCl_2$, 3 µM Na-orthovanadate, 1.2 mM DTT, 1 µM ATP/[γ-33P]-ATP), protein kinase (1-400 ng/50 µL) and TNK1 peptide (1 µM) were pipetted into 96-well, V-shaped polypropylene microtiter plates (assay plate). All PKC assays (except the PKC-mu and the PKC-nu assay) additionally contained 1 mM $CaCl_2$, 4 mM EDTA, 5 µg/ml phosphatidylserine and 1 µg/ml 1.2-dioleyl-glycerol. The MYLK2, CAMK1D, CAMK2A, CAMK2B, CAMK2D, CAMK4,

CAMKK2, and DAPK2 assays additionally contained 1 µg/ml calmodulin and 0.5 mM CaCl2. The PRKG1 and PRKG2 assays additionally contained 1 µM cGMP. One well of each assay plate was used for a buffer/substrate control containing no enzyme. The assay plates were incubated at 30°C for 60 minutes. Subsequently, the reaction cocktails were stopped with 20 µl of 4.7 M NaCl/35 mM EDTA. The reaction cocktails were transferred into 96-well streptavidin-coated FlashPlate® HTS PLUS plates (PerkinElmer, Boston MA), followed by 30 min incubation at room temperature on a shaker to allow for binding of the biotinylated peptides to the streptavidin-coated plate surface. Subsequently, the plates were aspirated and washed three times with 250 µl of 0.9% NaCl. Incorporation of radioactive ^{33}Pi was determined with a microplate scintillation counter (Microbeta, Perkin Elmer). For evaluation of the results of the FlashPlate® PLUS-based assays, the background signal of each kinase (w/o biotinylated peptide) was determined in parallel. 7 protein kinases were selected from the screen described above to repeat at three peptide concentrations (1 µM, 0.5 µM and 0.25 µM) in triplicate. The assays were performed as described above.

2.3.26. *In vitro IC50 of TP5801*

Compounds were tested at Reaction Biology in 10-dose IC50 mode with a 3-fold serial dilution in DMSO starting at 1-10 µM. Reactions were carried out at K_m ATP for each enzyme (5 µM for TNK1, 10 µM for Aurora A, 50 µM for ALK) and includes 33-P labeled ATP. Resulting % Enzyme activity (relative to DMSO controls) were plotted in GraphPad and IC50 values were determined by sigmoidal dose-response (variable slope) curve fits, bottom constraint of 0.

2.3.27. *NanoBRET Target Engagement Assay*

Transiently transfect TNK1-Nano-Luc Fusion vector DNA into HEK293 cells with FuGENE HD Transfection Reagent. After 24 hours, cells are transferred into 384-well NBS plates, where NanoBRET Tracer K5 reagent with final concentration of 0.125μM was delivered to cells. The cells were then incubated at 37ºC with 5% CO_2 for 1 hour. After incubation, the plate was removed from incubator and equilibrated to room temperature for 15 minutes. Complete substrate plus inhibitor were added to the cells. Cells were incubated at room temperature for 2-3 minutes. Donor emission wavelength (460nm) and acceptor emission wavelength (600nm) were measured using the Envision 2104 plate reader. Bret ratio is defined by acceptor sample divided by donor sample with background correction.

2.4. Results

2.4.1. *RNAi kinome screen identifies TNK1-dependence in a subset of hematological cancers.*

With the goal of identifying tyrosine kinase dependencies in primary cancers, 435 human patient samples were collected for *ex vivo* culture. These samples represented a variety of hematological cancers, including acute myeloid leukemia (AML), B-cell and T-cell acute lymphoblastic leukemia (ALL) and chronic myelogenous leukemia (CML). The samples were cultured and subjected to a high throughput RNAi screen of the tyrosine kinome, followed by cell viability assays (Supplemental. Figure 2-1A). RNAi targets that decreased cell viability by at least two standard deviations below the mean were scored as positive hits. 'Top hits' were defined as the kinase that, when depleted, had the largest negative impact on cell survival in a given sample. Predictably, among the most frequently identified top hits were well-described oncogenic tyrosine kinases, such as JAK1, JAK3, FLT3 and CSF1R. However, we unexpectedly identified TNK1 as

a top hit in a subset of ALL and AML samples (Supplemental. Figure 2-1B-C). Furthermore, in support of a link between TNK1 and ALL, we found a significant correlation between high TNK1 expression and decreased overall survival and relapse free survival in ALL patients (Supplemental. Figure 2-1D). Given a general lack of understanding of TNK1 function and regulation, we decided to probe deeper into TNK1 biology.

2.4.2. *Truncations reveal a cluster of phosphorylations within the proline rich domain that are required for 14-3-3 binding.*

To begin to uncover the function and regulatory mechanisms of TNK1, we identified TNK1-interacting proteins by BioID (BirA fused to the TNK1 C-terminus) and direct co-IP (FLAG-TNK1), followed by LC-MS/MS (Supplemental. Figure 2-2A-E). Both approaches revealed an abundance of the phospho-binding protein 14-3-3. Indeed, all 14-3-3 isoforms (β, γ, ε, ζ, θ, τ) except sigma were identified as putative TNK1-interacting partners from both approaches (Supplemental. Figure 2-2A). The TNK1-14-3-3 interaction was validated by co-IP and immunoblotting with a 14-3-3 antibody (Supplemental. Figure 2-2B). Furthermore, TNK1 failed to co-IP with a phospho-binding defective 14-3-3 (K49Q), indicating that the TNK1-14-3-3 interaction is mediated by phosphorylation(s) on TNK1 (Supplemental. Figure 2-2F).

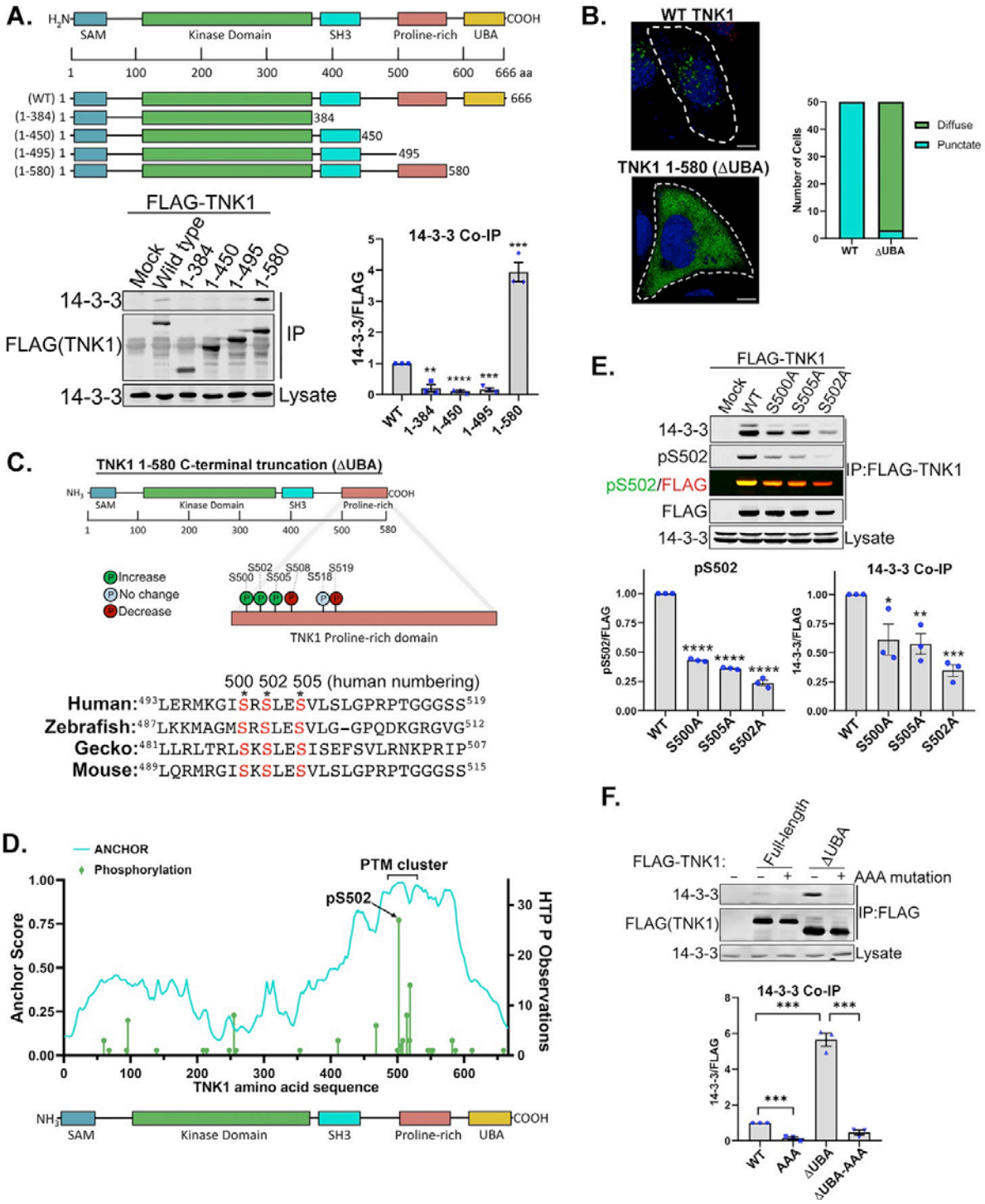

Figure 2-1. Phospho-Proteomics reveals a cluster of phosphorylations within the proline-rich domain of TNK1 and phosphorylation at S502 is required for 14-3-3 binding.

(A) Schematic diagram of wild type (WT) TNK1 and our panel of TNK1 truncations. FLAG-TNK1 (WT or indicated mutants) were immunoprecipitated from HEK-293T cells and immunoblotted for 14-3-3. Graph shows quantitation from multiple replicates with signals normalized to WT. Error bars represent SEM.

(B) HEK-293A cells expressing TNK1-GFP (WT or ΔUBA) were analyzed by confocal imaging for TNK1 localization. Graph shows number of cells, counted manually, with diffuse or punctate TNK1 localization (n=50).
(C) Schematic diagram of phosphorylations identified by TiO_2 phospho-proteomics within the proline-rich domain. Lower diagram shows an alignment of TNK1 sequence encompassing pS502 (human numbering) from human to zebrafish.
(D) Graph (green bars) shows the number of recorded observations of S/T phosphorylations on TNK1 via high-throughput methods (data derived from phosphosite.org) and the predicted disorder (cyan lines; ANCHOR score derived from https://iupred2a.elte.hu) across the sequence of TNK1.
(E) WT and mutant FLAG-TNK1 were immunoprecipitated from HEK-293T cells and immunoblotted for TNK1 phosphorylation at S502 and 14-3-3. Graphs show quantitation of infrared signal from multiple replicates with signals normalized to WT. Error bars represent SEM.
(F) WT and mutant FLAG-TNK1 were immunoprecipitated from HEK-293T cells and immunoblotted for 14-3-3. Graphs show quantitation of infrared signal from multiple replicates with signals normalized to WT. Error bars represent SEM.

To identify the phosphorylations on TNK1 that trigger 14-3-3 binding, we first put the TNK1 sequence through 14-3-3 site prediction algorithms (compbio.dundee.ac.uk/1433pred/), which predicted several candidate phosphorylation sites within loose 14-3-3 consensus motifs, including S60, S68, T392, S170, T401 and S434. However, none of the single S-to-A mutations at these sites had any measurable effect on 14-3-3 binding (selected mutants shown in Supplemental. Figure 2-3A). Therefore, we turned to deletion mapping, focusing first on known domains situated on the C-terminal side of the kinase domain, including the SH3, proline-rich and UBA domains. This approach mapped a 14-3-3-binding region to the proline-rich domain (Figure 2-1A). Interestingly, the UBA-deleted TNK1 construct (1-580 or "ΔUBA") not only retained 14-3-3 binding, but also showed an approximate 4-fold increase in interaction with 14-3-3 compared to WT TNK1 (Figure 2-1A). Furthermore, we noted that deletion of the UBA resulted in a markedly different localization pattern for TNK1—with WT TNK1 mostly forming large perinuclear puncta and TNK1 ΔUBA showing a diffuse cytosolic pattern (Figure 2-1B). Together,

these data were a first hint of interplay between the UBA domain and 14-3-3 binding, which we revisit further below.

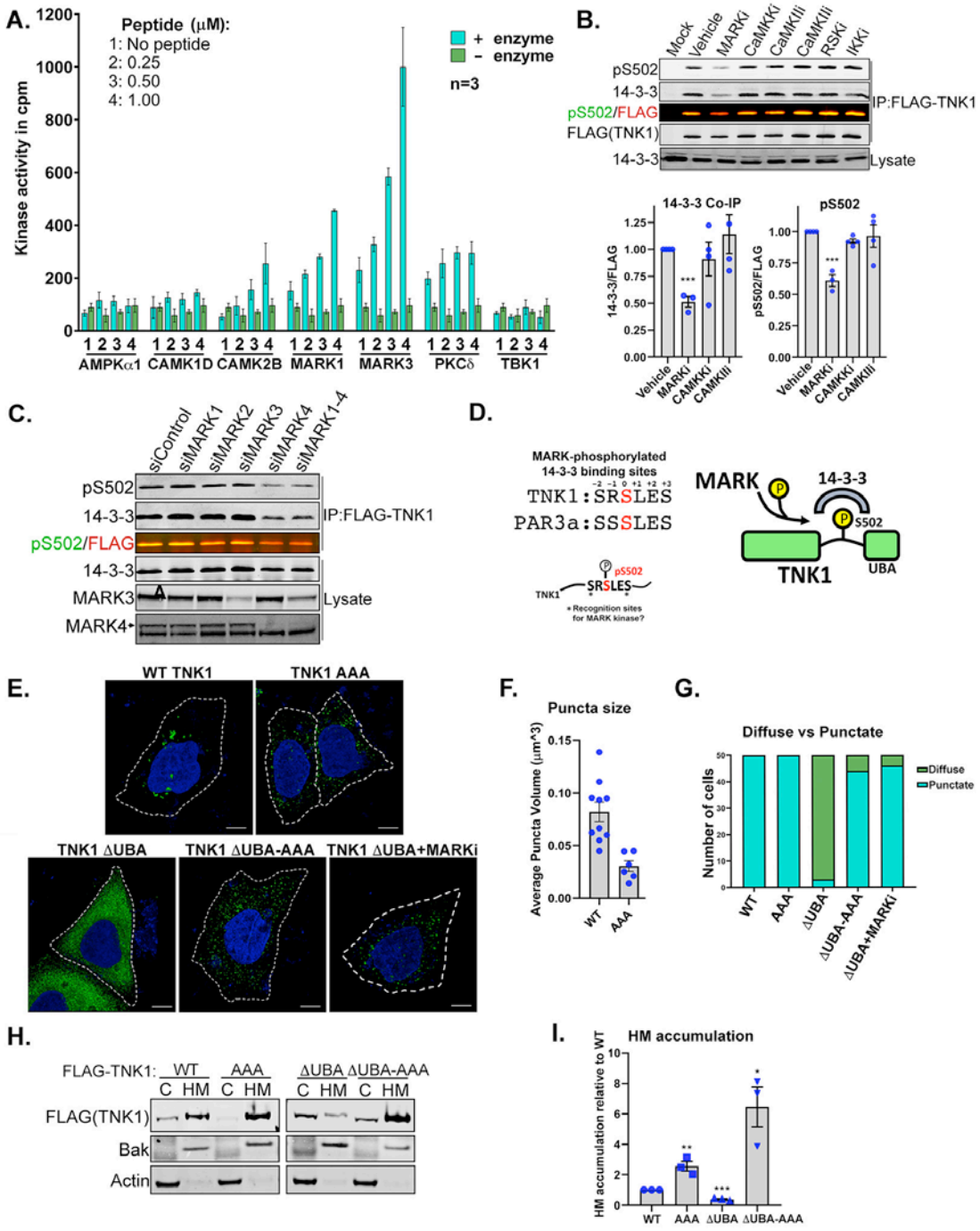

Figure 2-2. MARKs mediate TNK1 phosphorylation and 14-3-3 binding, which sequesters TNK1 away from cytosolic puncta.

(A) Radiometric protein kinase assays were performed to identify the kinase responsible for phosphorylation of TNK1 at S502. Corrected kinase activity (raw value minus sample peptide background) was measured in triplicate. Graph shows mean kinase activity in counts per minute (cpm) with error bar representing standard deviation.
(B) HEK293Ts expressing FLAG-TNK1 were treated with 1uM of indicated inhibitor for 4 hours (MARKi: MRT 67307 dihydrochloride, CaMKKi: STO-609, CaMKIIi: KN-92, KN-93, RSKi: LJI-308, IKKi: BMS 345541). FLAG-TNK1 was immunoprecipitated and blotted for pS502 and 14-3-3 binding. Graphs show quantitation normalized to WT TNK1. Error bars represent SEM.
(C) MARK kinases were depleted with siRNA (100nM) in A549 cells stably expressing FLAG-TNK1. FLAG-TNK1 was immunoprecipitated on FLAG resin and immunoblotted for pS502 and 14-3-3.
(D) (Left) Alignment of TNK1 sequence encompassing pS502 to a MARK-phosphorylated 14-3-3 binding site on PAR3a. (Right) Schematic model of MARK-mediated phosphorylation of TNK1 at S502 and 14-3-3 binding.
(E) HEK-293A cells express TNK1-GFP (WT or indicated mutants) were analyzed by confocal imaging for diffuse or punctate TNK1 localization and deconvolved with Hyugens software. TNK1 ΔUBA-expressing cells were treated with 1 uM MARK inhibitor (MRT 67307).
(F) Cells from panel E were analyzed for TNK1 puncta volume using Leica 3D analysis.
(G) Cells from panel E were scored for diffuse and punctate TNK1 localization as in figure 1B.
(H) HEK-293T cells expressing WT or the indicated mutants of FLAG-TNK1 were biochemically fractionated into cytosol and heavy membrane fractions, followed by immunoblotting for FLAG - TNK1. Fractions were also immunoblotted for Bak and actin as loading controls.
(I) The graph shows the relative HM/C ratio normalized to WT TNK1 from (H). Quantitation is from multiple replicates with error bar representing SEM.

First, given our co-IP results in Figure 2-1A, we reasoned that 14-3-3 docking site phosphorylations, likely within the proline-rich domain, should be elevated on TNK1 ΔUBA (1-580) compared to WT TNK1. As shown in Figure 2-1C, TiO_2 phospho-proteomics revealed a cluster of phosphorylations within the proline-rich domain at S500, S502 and S505 enriched on UBA-truncated TNK1. All three phosphorylations are catalogued at phosphosite.org as previously identified in high-throughput mass spectrometry (MS), but have no annotated function. Based on these unbiased aggregated MS studies, pS502 is the most frequently identified S/T phosphorylation across the entire sequence of TNK1 (Figure 2-1D). In addition, this cluster of phosphorylations lies within the region of TNK1 that scores highest for predicted disorder (Figure 2-1D), which suggests a protein-protein binding interface, particularly noted for other 14-3-3 binding sites [68-70].

We found that single S-to-A mutations at S500 and S505 partially reduce 14-3-3 binding to TNK1, whereas mutation at S502 had a more dramatic effect, reducing 14-3-3 binding to near-background levels (Figure 2-1E). 14-3-3 binding was completely eliminated by mutation of all three sites—referred to here as "TNK1 AAA" (Figure 2-1F).

We were initially puzzled by the requirement of such a tightly packed cluster of three phosphorylations for 14-3-3 binding. The phospho-binding groove of a 14-3-3 monomer only accommodates a single phosphorylation, and within a 14-3-3 dimer, the grooves are ~34 angstroms apart [48]. Initially, we reasoned that phosphorylations within this cluster may be required for phosphorylation at a distant 14-3-3 docking site. In this scenario, phospho-mimicking substitutions S500/502/505 should induce 14-3-3 binding. However, we found that S500E/S502E/S505E mutants are as effective at abrogating 14-3-3 binding as the phospho-null S-to-A mutations (Supplemental. Figure 2-3B), which is commonly observed for 14-3-3-docking site phosphorylations (Glu and Asp fail each to satisfy the chemistry of the 14-3-3 phospho-binding groove). We then questioned whether this cluster of three phosphorylations represents a non-canonical mode of 14-3-3 binding. In a FRET-based 14-3-3-binding assay, we only detected 14-3-3 binding to a mono-phosphorylated pS502 TNK1 peptide at levels comparable to our positive control, phospho-BAD (Supplemental. Figure 2-3C). Importantly, we did not detect any appreciable binding to the triple-phosphorylated pS500/pS502/pS505 peptide nor to a non-phosphorylated TNK1 peptide control (Supplemental. Figure 2-3C). Together, these data suggest that phosphorylation at S502 is sufficient for 14-3-3 binding in a canonical manner, but leave open the possibility of redundancy between the sites, a sequential requirement for phosphorylation at one site to precede another, or perhaps, most likely, that S500 and S505 are required for docking of the kinase to phosphorylate S502.

The sequence surrounding pS502 is a relatively poor match to consensus sequences of kinases commonly reported to phosphorylate 14-3-3 binding sites, such as PKB, PKC, AMPK and CAMKII [48]. Our targeted efforts to test these and other candidate kinases as regulators of pS502 did not reveal any compelling hits (data not shown). To expand our search, we generated a biotin-tagged peptide encompassing the S502 site and performed radiometric kinase assays with 245 individual human kinases that span the majority of Ser/Thr kinase subfamilies. Only two kinase subfamilies, Ca^{2+}/calmodulin-dependent kinases (CAMKs) and microtubule affinity-regulating kinases (MARKs), showed significant reactivity toward the S502 sequence, with MARKs as the top hit (Figure S3D-H and Figure 2A). Subsequent kinase inhibitor experiments in cells indicated that MARKs, but not CAMKII, phosphorylate S502 (Figure 2-2B).

MARKs (MARK1-4) are members of the AMPK family and, like AMPK, are activated downstream of the tumor suppressor LKB1 [71, 72]. They were initially named for their role in regulating microtubule dynamics to control dendrite growth and cell motility [73]. Genetic studies indicate some redundancy among the different MARKs[74] and, importantly, some MARK substrates have been shown to interact with 14-3-3 [75, 76]. For example, the phosphorylation site that mediates 14-3-3-binding on one MARK substrate, Par3a, is similar to the sequence surrounding pS502: KSS[pS]LES on Par3a compared to ISR[pS]LES on TNK1—both of which differ from the loose consensus for 14-3-3 binding sites with neither an Arg nor Pro in the -3 and +2 positions, respectively [48]. To test this idea further, we depleted cells of individual MARK isoforms and found that knockdown of MARK4 reduces pS502 and 14-3-3 binding to TNK1 (Figure 2-2C-D).

2.4.3. *Phosphorylation of TNK1 and 14-3-3 binding restrain the movement of TNK1 into heavy membrane-associated clusters.*

To begin to understand what effect the MARK-mediated 14-3-3 interaction has on TNK1, we compared the localization of WT and AAA mutant TNK1. Confocal imaging showed that loss of 14-3-3 binding, caused by the AAA mutation, triggers TNK1 to consolidate into punctate structures within the cytosol (Figure 2-2E-G). This effect is particularly pronounced with TNK1 ΔUBA, which moves dramatically from diffuse to punctate upon mutation of the 14-3-3 docking site (Figure 2-2E and G). Importantly, we found that inhibition of MARK kinase activity completely reproduced the effect of the AAA mutation in causing TNK1 ΔUBA to contract into distinct cytosolic puncta (Figure 2-2E and G), further supporting the idea that MARKs govern TNK1 via phosphorylation at S502 and consequent control of 14-3-3 binding.

In an effort to validate our confocal imaging observations through biochemical methods, we found that the bulk of WT TNK1 was found in a 1% Triton X-100-soluble heavy membrane (HM) fraction. In contrast, deletion of the UBA shifted TNK1 into the cytosolic (C) fraction (Figure 2-2H-I), reflecting the diffuse pattern of localization observed by confocal imaging (Figure 2-2E). Remarkably, consistent with imaging data in figure 2E, disruption of 14-3-3 binding caused an accumulation of full-length TNK1 and TNK1 ΔUBA in the HM fraction. Together, these data suggest that MARK-mediated phosphorylation of TNK1 and 14-3-3 binding sequester TNK1 in the cytosol, preventing TNK1 movement into heavy membrane-associated clusters.

2.4.4. *TNK1 contains a high affinity UBA domain that interacts with multiple ubiquitin linkages.*

These initial observations—that deletion of the TNK1 UBA domain increases TNK1 interaction with 14-3-3 and affects its localization— led us to investigate the TNK1 UBA. To the best of our knowledge, TNK1 and ACK1 are the only known human tyrosine kinases with predicted UBA domains. Thus, we questioned whether the TNK1 UBA acts conventionally,

through binding ubiquitin, or plays some other ubiquitin-independent role in kinase regulation (e.g., like AMPK UBAs). As shown in Figure 2-3A, WT TNK1 co-immunoprecipitated from cells with a range of ubiquitinated species, which were lost with TNK1 ΔUBA, suggesting that TNK1 has a functional UBA domain.

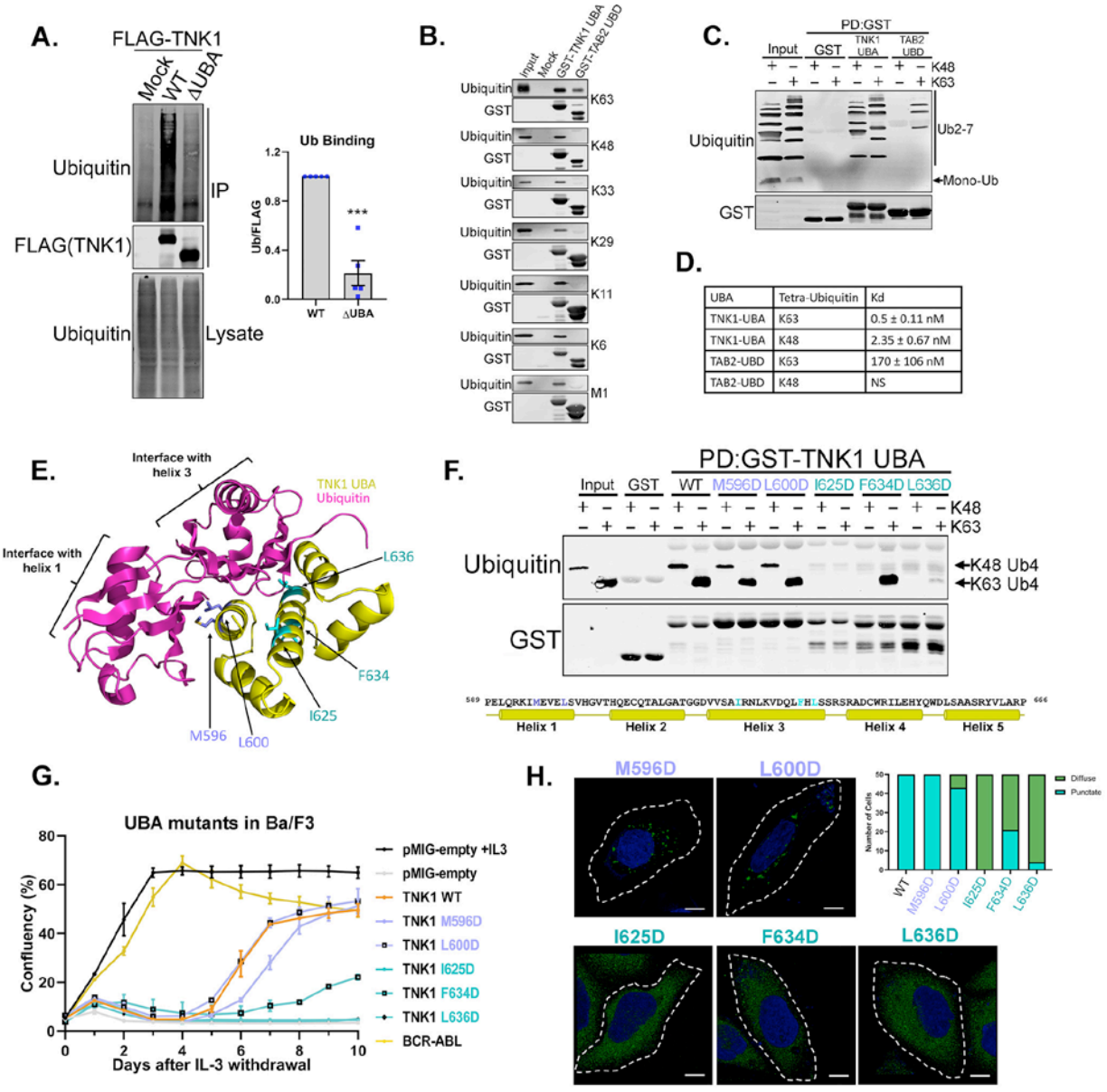

Figure 2-3. TNK1 possesses a functional UBA at its C-terminus and the ubiquitin binding properties of the TNK1 UBA are essential for TNK1 activity and TNK1-driven cell proliferation.

(A) WT or ΔUBA FLAG-TNK1 were immunoprecipitated from HEK-293T cells and immunoblotted for ubiquitin binding. Graphs show quantitation from multiple replicates with signals normalized to WT. Error bars represent SEM.
(B) Recombinant GST-TNK1-UBA or GST-TAB2-UBD were incubated with individual tetra-ubiquitin chains of various linkages at 4ºC for 2 hours. GST-tagged proteins were captured on glutathione resin and immunoblotted for GST and ubiquitin.

(C) Recombinant GST-TNK1-UBA or GST-TAB2-UBD were incubated with a cocktail of mono-ubiquitin together with either K48- or K63-linked poly-ubiquitin of chain lengths 2-7. Captured GST-proteins were immunoblotted as in panel B.
(D) A table summary showing average measured Kd of TNK1-UBA/TAB2 UBD towards K48/K63 linked tetra-ubiquitin using Bio-layer interferometry (BLI). Errors representing standard deviation of the measured Kd.
(E) The diagram shows a Rosetta-modeled structure of TNK1 UBA domain and a homology model-based prediction of the binding interfaces between the UBA and ubiquitin.
(F) Recombinant GST-tagged WT and mutant TNK1 UBA were incubated with either K48 or K63 tetra-ubiquitin. The GST-UBA was captured and immunoblotted as in panel B.
(G) Ba/F3 cells were transduced with retrovirus expressing either the pMIG-empty vector, WT TNK1, the indicated TNK1 mutants or BCR-ABL. IL-3 independent growth was monitored by IncuCyte live cell imaging. Error bars represent SEM.
(H) Confocal analysis of TNK1-GFP (WT or indicated mutants) in HEK-293A cells as in figure 2-1 panel B.

To test the ubiquitin binding specificity of the TNK1 UBA in a cell free system, we produced a GST-tagged recombinant TNK1 UBA and measured its binding to various linkages of tetra-ubiquitin (K6-, K11-, K29-, K33-, K48-, K63- and M1-linked). The TNK1 UBA interacted with all linkage types tested (figure 2-3B). As a control, a GST-tagged ubiquitin-binding domain from TAB2 (TAB2 UBD) showed specificity for K63-linked chains (figure 2-3B), as previously reported[77]. Next, we took advantage of the different electrophoretic mobilities of K48-, K63- and M1-linked chains and measured their binding to TNK1 UBA in a mixed, competition-based pull-down assay. Again, the TNK1 UBA showed no apparent preference for linkage type, whereas the TAB2 UBD selectively pulled down K63-linked ubiquitin from the mixture (sup. figure 2-4A). We also observed robust interaction between the TNK1 UBA and K63- or K48-linked poly-ubiquitin of variable chain lengths (Ub2-7), but were unable to observe any interaction with mono-ubiquitin (figure 2-3C).

Despite adding equimolar concentrations of ubiquitin chains to the pulldown assays in figures 2-3C and sup. figure 2-4A, their interpretation by immunoblot is complicated because ubiquitin antibodies often show preference for K63-linked chains[77]. Therefore, we analyzed the GST-tagged TNK1 UBA and TAB2 UBD by biolayer interferometry (BLI) with purified K48- and K63-linked tetra-ubiquitin chains to measure dissociation constants (Kd). For the TNK1 UBA, we observed a Kd of 0.5 nM for K63-linked ubiquitin and a comparatively lower affinity for K48-linked ubiquitin with a Kd of 2.35 nM (figure 2-3D and sup. figure 2-4B). Both affinity measurements place the TNK1 UBA at the lower range of observed dissociation constants for UBA domain interactions with tetra-ubiquitin [78-80], indicating a tight interaction between the TNK1 UBA and structurally diverse ubiquitin linkages. For comparison in our assays, the TAB2 UBD showed a Kd of 170 nM for K63-linked ubiquitin—similar to the previously published Kd for TAB2 UBD[81] — but had no detectable affinity for K48-linked chains (figure 2-3D and sup. figure 2-4B).

To further characterize the TNK1 UBA and develop tools to understand the relationship between ubiquitin binding, 14-3-3 binding and TNK1 kinase activity, we looked for residues within the TNK1 UBA that interface with ubiquitin. There is no published crystal structure of full-length TNK1 and our attempts to purify TNK1 were unsuccessful, likely due to a large region of predicted intrinsic disorder between the SH3 domain and the UBA. Computational modeling of the TNK1 UBA domain suggests homology between the TNK1 UBA and published crystal structures of other UBA domains. Therefore, we submitted the putative TNK1 UBA domain amino acid sequence (residues 590 - 666) to the Robetta server for structure prediction via Rosetta homology modeling [82]. The closest match, according to primary sequence and predicted secondary

structure, is the UBA domain of the ubiquitin-associated protein 1 (UBAP1) subunit of ESCRT-I, a seven-helix bundle [83].

Our homology modeling (see materials and methods for details) suggested potential ubiquitin-binding interfaces within helices 1 and 3 of the TNK1 UBA (Figure 2-3E). However, point mutations in helix 1 at M596 and L600 had no effect on TNK1-ubiquitin binding. In contrast, mutations at I625 and L636 in helix 3 abolished the interaction with ubiquitin. Notably, a mutation at F634, also within helix 3 (but not predicted to directly interface with ubiquitin in our model), disrupted the interaction with K48-linked ubiquitin, but had no effect on K63-linked chains (Figure 2-3F).

The uniqueness of a kinase possessing a high-affinity and indiscriminate UBA domain raised our interest in the role the UBA might play in regulating TNK1 kinase activity. TNK1 was previously identified in a retroviral screen for tyrosine kinases that transform the normally IL-3-dependent pro-B cell line, Ba/F3, to growth factor independence[31]. Consistent with their results, we found that retrovirus-expressed WT TNK1 transformed Ba/F3s to IL-3-independence within 5-7 days (Figure 2-3G). However, the helix 3 mutations that completely disrupted ubiquitin binding, abolished TNK1-mediated transformation of Ba/F3s, whereas F634D, which only partially inhibited ubiquitin binding, likewise partially delayed transformation (Figure 2-3F-G). Consistent with these results, we found that any mutation that disrupts ubiquitin binding also reduces TNK1 kinase activity, as measured by global phospho-tyrosine levels (Supplemental. Figure 2-4C, quantitation in Supplemental. Figure 2-4E). Furthermore, the loss of ubiquitin binding and TNK1 activity correlated with increased binding of TNK1 to 14-3-3 and a diffuse localization across the cytosol (Figure 2-3H and Supplemental. Figure 2-4D), which is consistent with what we observed for TNK1 ΔUBA (Figure 2-1A-B). As quantified in Figure S4E, this

inverse relationship between 14-3-3 binding and TNK1 activity suggests that phosphorylation at S502 and 14-3-3 binding may inhibit TNK1 kinase activity.

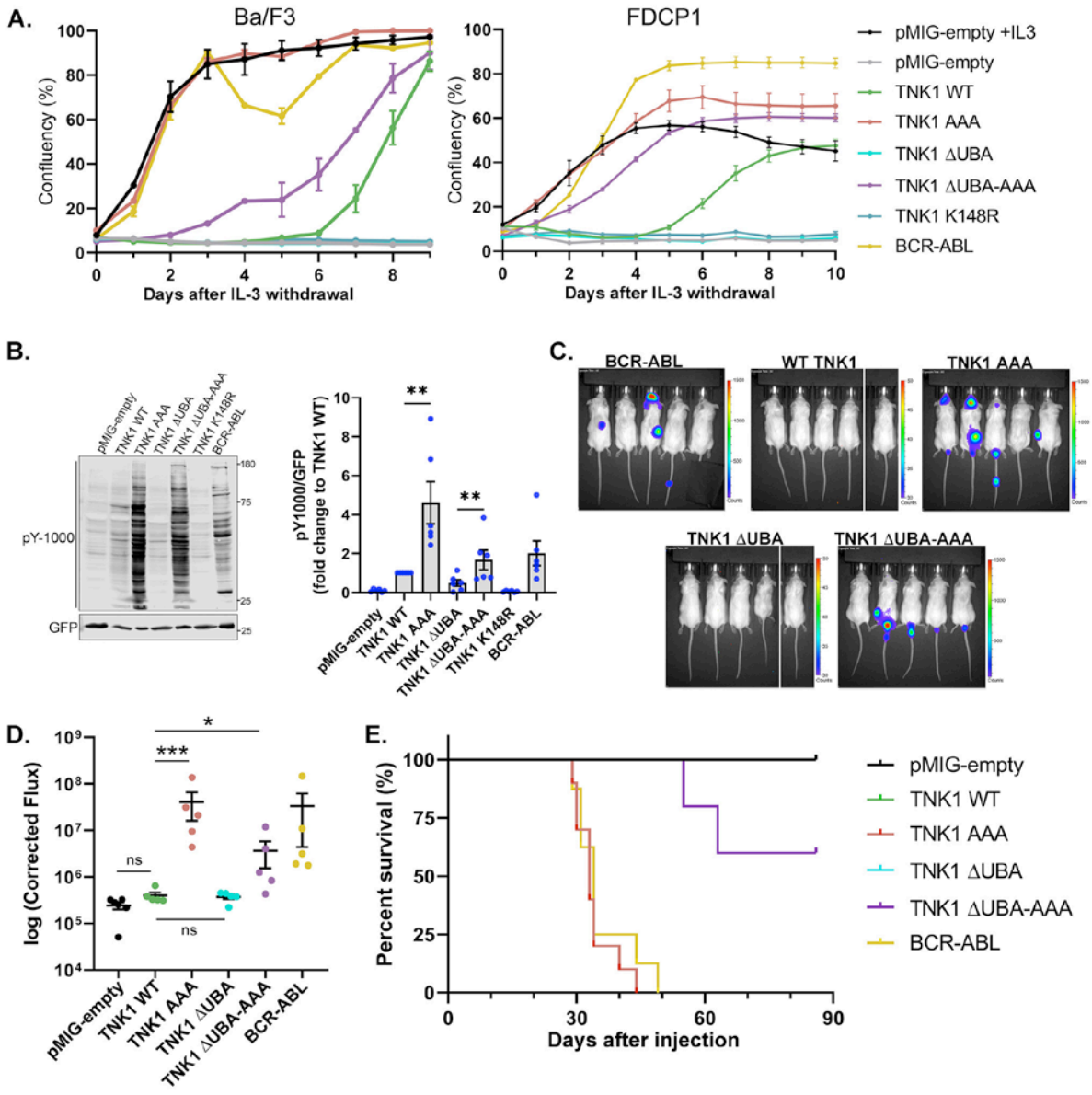

Figure 2-4. Loss of 14-3-3 binding activates TNK1 and unleashes TNK1-driven tumor growth in vivo.

(A) Ba/F3 or FDCP1 cells were transduced (as in Figure2- 4) with either pMIG-empty vector, TNK1 (WT or indicated mutants) or BCR-ABL. IL-3 independent growth was monitored as in Figure 2-3 panel G.

(B) Ba/F3 cells from panel A were immunoblotted for global phospho-tyrosine and GFP. Graphs show global tyrosine phosphorylation quantitation from multiple replicates with signals normalized to WT. Error bars represent SEM.

(C) $1x10^6$ Ba/F3-luc cells transduced with WT TNK1 or the indicated TNK1 mutants were injected into the tail vein of NOD/SCID mice. Luminescent signal was imaged and quantified using IVIS imaging and ROI analysis. Images shown are mice in prone position 28 days after injection.
(D) Corrected Flux (raw luminescent signal minus background luminescent signal) of mice from panel C.
(E) Survival plot of mice from panel C.

2.4.5. *Full activation of TNK1 requires release from 14-3-3 and interactions between the TNK1 UBA and ubiquitin.*

To begin to disentangle the effect of 14-3-3 and ubiquitin binding on TNK1 activity, we transduced Ba/F3 cells and a similarly IL-3-dependent myeloid progenitor line, FDC-P1, with retroviruses expressing our panel of TNK1 mutants, including the 14-3-3-binding-defective TNK1 AAA mutant, followed by measurement of growth factor independence as in Figure 2-3G. The potently oncogenic BCR-ABL served as a positive control[84] . Remarkably, the TNK1 AAA mutant induced growth factor independence almost immediately after IL-3 withdrawal, which was comparable to the rapid transformation observed with BCR-ABL, both of which transformed cells several days ahead of WT TNK1 (Figure 2-4A). This effect of TNK1 on Ba/F3s was completely dependent on kinase activity, as a kinase-dead point mutation (K148R) abolished transformation (Figure 2-4A).

Consistent with our observation that UBA-disrupting point mutations inhibit TNK1 activity, we found that TNK1 ΔUBA failed to promote growth factor independence (Figure 2-4A). Interestingly, the combination of UBA deletion and AAA mutation only resulted in delayed kinetics of transformation compared to the AAA mutation alone, yet it was still significantly more potent than WT TNK1 in these assays (Figure 2-4A). The rate of transformation by each mutant tracked with TNK1 kinase activity, such that TNK1 AAA showed the highest levels of global phospho-tyrosine, while deletion of the UBA resulted in lower activity for WT TNK1 and the

AAA mutant (Figure 2-4B). Nevertheless, TNK1 ΔUBA-AAA promoted significantly higher levels of global phospho-tyrosine than TNK1 ΔUBA alone (Figure 2-4B). These results support the idea that release of TNK1 from 14-3-3 is the critical step toward TNK1 activation and that interactions between the UBA domain and ubiquitin, although important, play a secondary role in driving TNK1 activity (see discussion for more detail).

The Hodgkin lymphoma (HL) cell line L540 carries a paracentric chromosomal inversion that truncates TNK1 at D472, generating an active and highly expressed form of TNK1 [32]. Because this truncation occurs just N-terminal to S502, it effectively eliminates the 14-3-3 binding site and UBA, which yields a TNK1 protein similar to our TNK1 ΔUBA-AAA construct—both lacking the 14-3-3 and UBA motifs. Indeed, expression of a D472-truncated TNK1 promotes growth factor-independence in Ba/F3 cells with similar kinetics to TNK1 ΔUBA-AAA (Supplemental. Figure 2-5A-B, compare to Figure 2-4A). Thus, our data provide a mechanistic explanation (i.e., loss of 14-3-3 binding) for why this naturally occurring truncation generates an active, oncogenic form of TNK1.

To measure the ability of TNK1-driven Ba/F3 cells to grow *in vivo*, we stably integrated luciferase into the parental Ba/F3 cells for bioluminescent imaging of tumor burden, followed by retroviral expression of our panel of TNK1 variants and BCR-ABL. In a murine model, in which mice were injected with Ba/F3 cells via the tail vein, we found that TNK1-AAA-driven cells established rapid tumor burden and induced mortality with similar kinetics to BCR-ABL (Figure 2-4C-E). In contrast, mice injected with WT- and TNK1 ΔUBA-expressing cells showed no detectable tumors nor physical signs of tumor burden (Figure 2-4C-E). Interestingly, TNK1 ΔUBA-AAA cells established low levels of tumor burden, but cells were primarily confined to the tail (Figure 2-4C) and were remarkably benign in this model (Figure 2-4D-E).

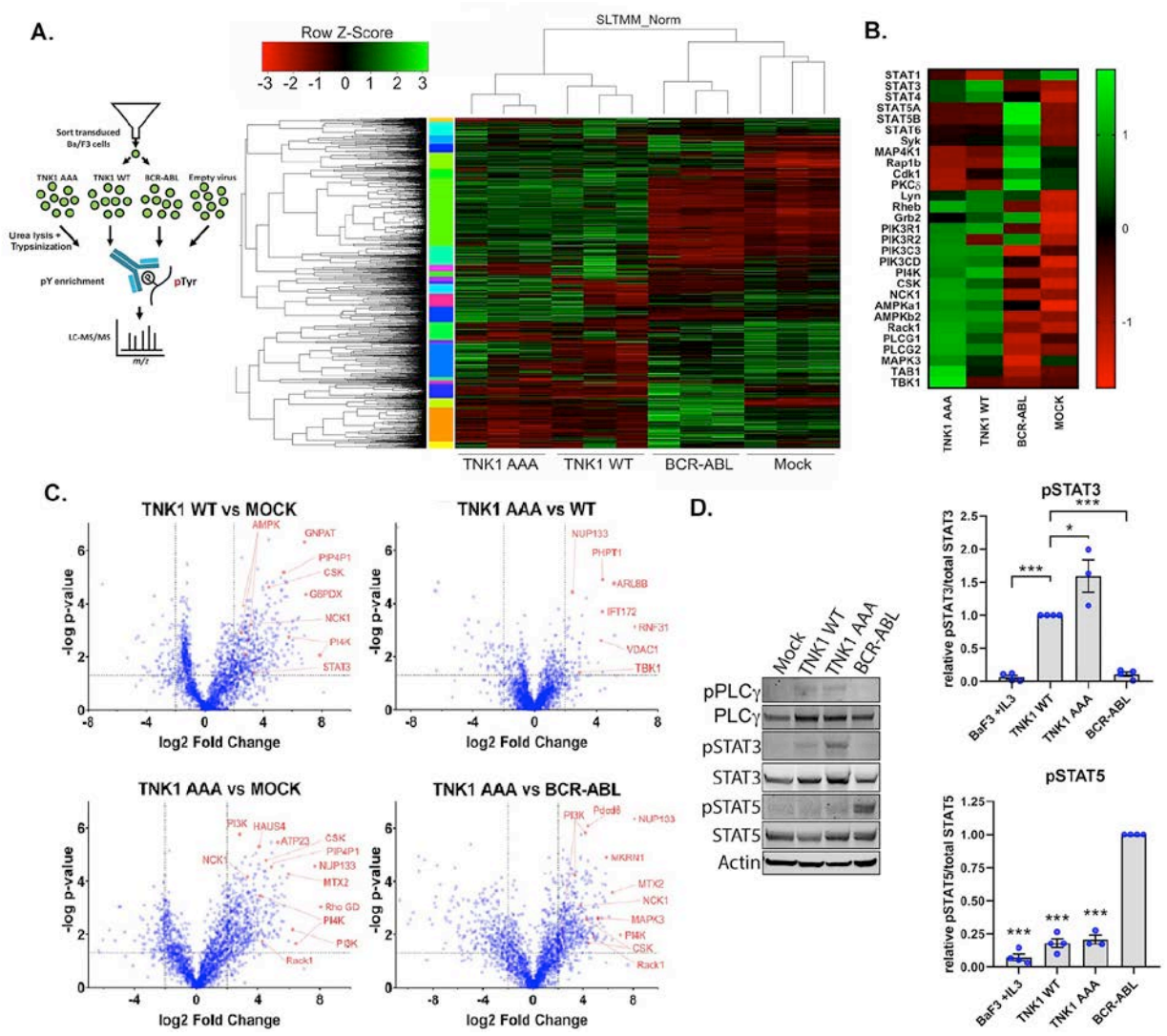

Figure 2-5. Quantitative phospho-tyrosine proteomics reveals a TNK1-mediated network of phospho-substrates.

(A) (Left) Schematic illustration of experimental design for phospho-tyrosine proteomics. (Right) Heat map shows the hierarchical clustering analysis of all 2,294 phospho-tyrosine peptides from three biological replicates of each sample.

(B) A focused heat map showing the relative phospho-tyrosine signal of selected significant substrates across the different samples.

(C) Volcano plots of phosphorylation changes between the indicated samples. Selected phospho-substrates are highlighted in red.

(D) Indicated Ba/F3 cells were immunoblotted for phosphor-PLCγ1 (Y284), total PLCγ1, phosphor-STAT3 (Y705), total STAT3, phosphor-STAT5 (Y694), total STAT5 and β-actin. Graphs show quantification from multiple replicates. Phosphorylation signals were normalized to respective total protein signals. pSTAT3/STAT3 signals were normalized to TNK1 WT. pSTAT5/STAT5 signals were normalized to BCR-ABL. Error bars represent SEM.

2.4.6. *Phospho-tyrosine proteomics reveals a network of TNK1-mediated phospho-substrates.*

The ability of TNK1-AAA and BCR-ABL to induce rapid growth factor-independence *in vivo*, suggested they may be functioning through similar pathways despite differences in domain architecture. The Ba/F3 cells provided a relatively clean isogenic system to evaluate the phospho-tyrosine substrate networks of these kinases with minimal noise from other tyrosine kinases after IL-3 withdrawal (Figure 2-5A, experimental layout). Thus, to determine phospho-tyrosine substrate networks for these kinases, we performed phospho-tyrosine enrichment and quantitative LC-MS/MS. We found that WT TNK1 and TNK1-AAA showed similar phospho-tyrosine profiles, but were markedly different than BCR-ABL, which can be visualized in the global phospho-tyrosine heat map (Figure 2-5A). Indeed, an opposite phospho-tyrosine fingerprint emerged for TNK1, relative to BCR-ABL, across a number of proteins, including multiple PI3K subunits, PI4K, AMPK subunits, PLC-γ, TAB1, TBK1, NCK1, Rack1, STATs and others (Figure 2-5B). In addition, for TNK1 AAA relative to TNK1 WT, we saw an enrichment of phospho-tyrosine substrates involved in ubiquitin processes (Supplemental. Figure 2-6A-B)[85]. Pairwise comparisons of the kinases or kinases to mock are shown by volcano plot in Figure 2-5C.

Next, we selected a subset of phospho-tyrosine substrates from the proteomics data for validation. An early study on TNK1 identified Phospholipase C-gamma (PLC-γ) as a TNK1 interacting partner, but the interaction had no clear function[28]. As shown in figure 2-5E, we found that TNK1, but not BCR-ABL, phosphorylates PLC-γ at Y783, a phosphorylation known to activate PLC-γ enzymatic activity while in complex with growth factor receptors [86, 87]. Another potentially interesting divergence between TNK1 and BCR-ABL lies in STAT3 and STAT5 (see Figure 2-5B, STAT panels). Consistent with the proteomics data, we found that TNK1 promoted

an activating phosphorylation of STAT3, but not STAT5. Conversely, BCR-ABL triggered phosphorylation of STAT5, but not STAT3 (Figure 2-5D). Accordingly, inhibition of STAT3 by the clinical STAT3 inhibitor Niclosamide [88] blocked TNK1-driven cell growth, but had little effect on BCR-ABL-driven growth (Supplemental. Figure 2-6C).

2.4.7. *Development of a TNK1 inhibitor.*

Collectively, our data implicated TNK1 as a potential therapeutic target. To identify candidate anti-TNK1 compounds, we screened small molecule libraries for compounds with activity against recombinant TNK1 in biochemical assays (Supplemental. Figure 2-7A). An experimental compound, TP-5801, was designed based on initial hits in our biochemical screen. TP-5801 aligns along the hinge of the protein, with the aryl bromo substituent orienting towards the gate-keeper methionine residue. A single hydrogen bond is shown between the N1 of the pyrimidine ring of TP-5801 and the backbone NH of L198 hinge residue. Major hydrophobic interactions occur between the sidechain of L122, the backbone of G202 and the substituted phenyl ring of TP-5801. The substituted pyridine ring of TP-5801 situates beneath the P-loop with the dimethylamino group oriented towards the catalytic lysine, forming major hydrophobic interactions with the sidechains of L252 (P-loop) and V130 (Figures 2-6A, Supplemental. Figure 2-7B). In vitro assays with purified kinases revealed IC50s of 1.40 nM against TNK1 compared to 5.38 uM against Aurora A kinase (Figure 2-6B). Nano-BRET analysis of TP-5801 indicated an IC50 of 10.5 nM against TNK1 (Supplemental. Figure 2-7C). To transition to a cell-based system, we used the TNK1-driven and BCR-ABL-driven Ba/F3 cell pair, which we verified to have differential kinase dependency using the BCR-ABL inhibitor asciminib (Supplemental. Figure 2-7D). In Ba/F3 cells, TP-5801 potently inhibited TNK1-driven cell growth with IC50s of 77.8 and 37.0 nM against WT TNK1 and AAA mutant cells, respectively (Figure 2-6C). For comparison in

the same model, TP-5801 inhibited BCR-ABL-driven and IL3-driven Ba/F3 cell growth with IC50s of 8.5 and 1.2 μM respectively (Figure 2-6C, see Figure 2-6E for summary of IC50s). Furthermore, as we would predict, low nM levels of TP-5801 blocked the growth of the TNK1-dependent HL cell line, L540 (Figure 2-6D).

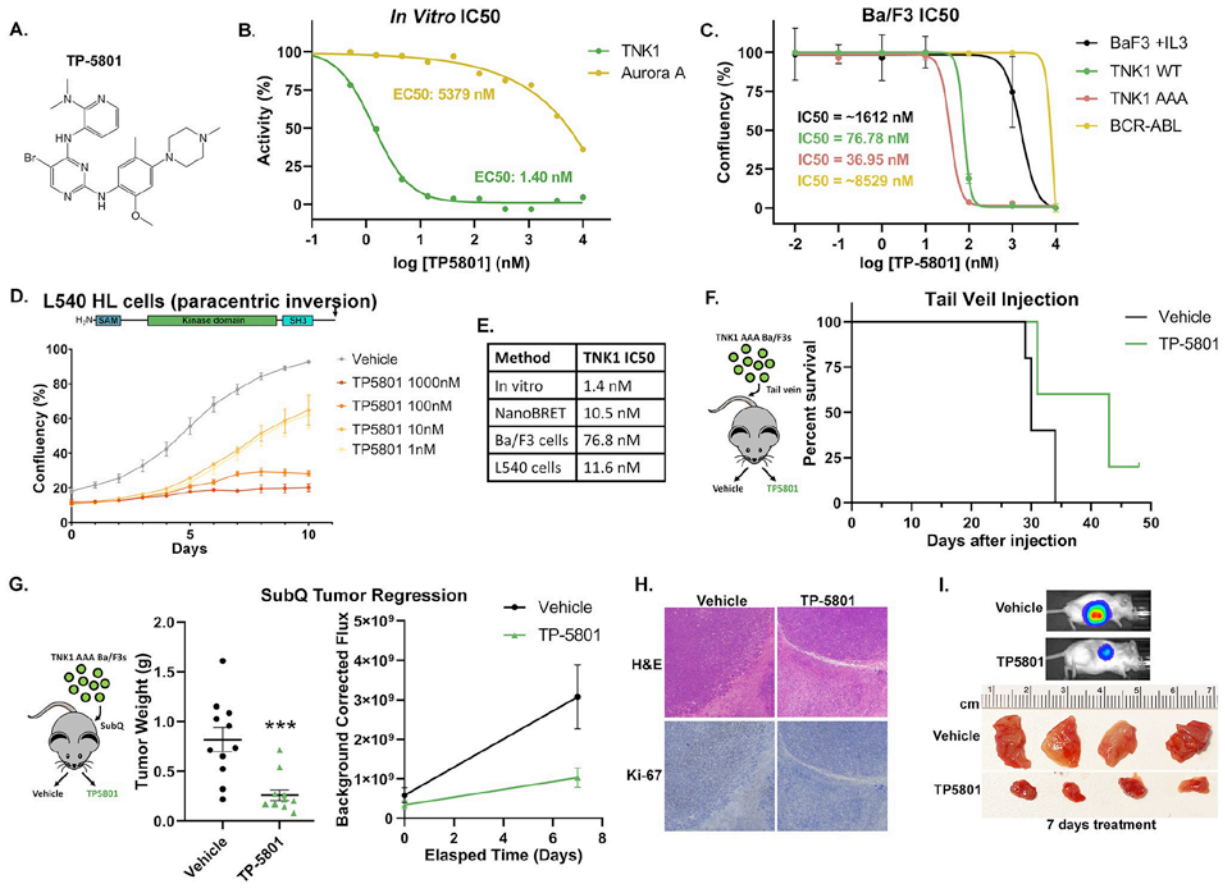

Figure 2-6. The development of a potent TNK1 inhibitor that reduces tumor burden and extends life span in a TNK1-driven tumor model.

(A) The structure of TP-5801.
(B) In vitro IC50.
(C) IC50 graph of IL3 driven Ba/F3 cells, TNK1-WT/AAA driven Ba/F3 cells or BCR-ABL-driven Ba/F3 cells treated with TP-5801(10pM to 10mM) for 72 hours. Cell confluency was measured using IncuCyte imaging system.
(D) Schematic diagram showing the truncated from of TNK1 as a result of paracentric inversion in L540 cells. L540 cells were treated with the indicated doses of TP-5801 or vehicle (DMSO) and analyzed for cell growth in an Incucyte live-cell growth chamber.
(E) Table summary of the IC50 values of TP-5801 obtained by different methods.

(F) TNK1-AAA driven Ba/F3-luc cells were injected into the tail veil of NOD/SCID mice. The mice were treated once daily by oral gavage with either vehicle or TP-5801 (10mg/kg).
(G) NOD/SCID mice were subcutaneously injected with TNK1-AAA driven Ba/F3-luc cells. Once tumor size reached 150-250mm3, mice were treated once daily by oral gavage with either vehicle or 50mg/kg TP-5801 for seven days. Luminescent signal was imaged and quantified using IVIS imaging. Mice were euthanized after a one-week treatment and tumors were resected and weighed.
(H) Formalin fixed and paraffin-embedded tumor tissue from the indicated mice were immunostained for the proliferative nuclear antigen Ki-67 and counterstained with hematoxylin and eosin (H&E).
(I) Images show the luminescent signal from panel G and the resected tumors after one week of treatment.

Next, we evaluated the efficacy of TP-5801 in the mouse survival model from Figure 4, in which TNK1-AAA cells were injected intravenously. In this model, daily oral administration of TP-5801 at 10 mg/kg significantly prolonged lifespan compared to vehicle-treated mice (Figure 2-6F). To assess the impact of TP-5801 on localized tumor growth, we used a subcutaneous xenograft model. After 1 week of treatment, TP-5801 induced significantly more tumor regression (Figures 2-6G-I). Together, these data elucidate a lead compound, TP-5801, as an anti-TNK1 small molecule.

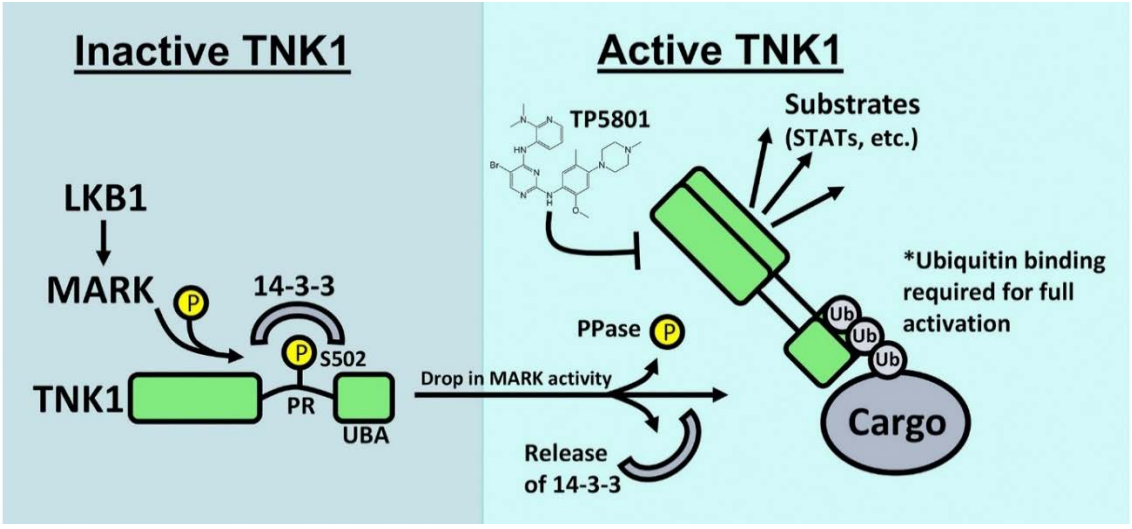

Figure 2-7. A model of TNK1 regulation showing the contribution of MARK-mediated 14-3-3 binding and the unique contribution of the TNK1 UBA to kinase activation.

Our data suggest that 14-3-3 restrains TNK1 activity by preventing its clustering into cytosolic membrane-associated puncta, in which TNK1 is active. Once released from 14-3-3, interactions between TNK1 and ubiquitin are essential for full TNK1 activity. Mutations that disrupt 14-3-3 binding activate TNK1, rendering it capable of driving rapid growth factor independence and tumor growth in vivo. Also shown is the small molecule TP-5801, which inhibits TNK1 at low nM levels and blocks TNK1-driven tumor growth in vivo.

2.5. Discussion

Our data suggest a two-step mechanism to explain how TNK1 becomes active: First, TNK1 kinase activity is unleashed by release of 14-3-3. Second, interactions between ubiquitin and the C-terminal TNK1 UBA allow for full activation of TNK1 (Figure 2-7). To our knowledge, this is the first example of a kinase possessing a functional ubiquitin-binding domain and relying on ubiquitin binding for full activation. This concept of UBA involvement in TNK1 activation raises interesting questions about the interplay between 14-3-3 and the UBA and exactly how the UBA contributes to TNK1 activity at a structural level.

Tyrosine kinases are often activated through oligomerization, which occurs through various forms of induced proximity/clustering [6, 89]. For TNK1, our imaging data suggest that 14-3-3 controls clustering. This is most easily seen comparing the cellular distribution of TNK1 ΔUBA, which interacts heavily with 14-3-3 (note 14-3-3 IP in Figure 2-1), and the 14-3-3 binding-null TNK1 ΔUBA-AAA (Figure 2-2E). These data show that loss of 14-3-3 binding induces a marked clustering of TNK1 into cytosolic puncta (Figure 2-2E). Our biochemical data suggest that this clustering within a heavy membrane-associated fraction (Figure 2-2H-I). Thus, the release of 14-3-3 may concentrate TNK1 at membrane-associated puncta, while interactions between the UBA and ubiquitinated species within these clusters may help to align TNK1 monomers for optimal oligomerization. It is also possible that the UBA may home or tether TNK1 to substrates. It is notable that TNK1 ΔUBA-AAA-driven Ba/F3 cells, although highly proliferative, failed to

migrate outside the tail, suggesting that the UBA may home TNK1 to substrates that promote cell migration and invasion. In support of this idea, we identified a variety of putative TNK1 substrates involved in motility and ubiquitin-related processes (Supplemental. Figure 2-2D and Supplemental. Figure 6).

Our studies in IL-3-dependent B cell lines show that although truncation of the UBA from TNK1 AAA diminished its activity relative to TNK1 AAA alone, it was still more active than WT TNK1 (Figure 2-4). This was initially puzzling based on our notion that the UBA is necessary for TNK1 activity (Figure 2-3G). However, at least two other observations provide some additional insight: First, we consistently found that deletion of the UBA increased the levels of TNK1 protein, which suggests the UBA may ultimately target TNK1 for degradation, perhaps by tethering TNK1 to cargo destined for the proteasome or lysosome. Second, our imaging data, mentioned above (Figure 2-2E), indicate that 14-3-3 plays a dominant role in controlling the clustering of TNK1 at cytosolic puncta. Taken together, these two effects (increased stability and clustering) may simply result in a high enough local concentration of TNK1 ΔUBA-AAA at the cytosolic puncta to promote oligomerization and activation, even in a less-than-optimal condition (lacking the UBA).

The only other member of the human ACK kinase family, ACK1, is more studied than TNK1. ACK1 is activated downstream of receptor tyrosine kinase signaling, promotes androgen receptor expression, and directly drives EGFR recycling after EGF stimulation [9, 14, 15, 18, 19]. Curiously, nearly all of what is known about ACK1 function/regulation involves domains that are absent in TNK1. The clathrin-binding domain, the Cdc42/Rac-interacting domain and the Mig6-homology domain of ACK1 are all absent in TNK1, which in turn largely accounts for the shorter sequence of TNK1. We posit that the regulatory void left by the absence of these domains in TNK1 is essentially filled by the 14-3-3 regulatory motif. This also suggests functional divergence

between these kinases and raises interesting evolutionary questions. Why has selective pressure maintained the core kinase domain, SH3 domain and UBA domain of TNK1 and ACK1, but driven divergence outside these domains? Have the ubiquitin-binding properties of the TNK1 and ACK1 UBA diverged? And in the bigger picture, how different are the biological functions of these kinases?

Another question relates to the clinical significance of TNK1 as a therapeutic target. We began this study with the identification of TNK1 as an essential tyrosine kinase in a subset of hematological cancers. Previous studies on TNK1, while limited in number, have been mixed—with some suggesting a tumor suppressive function and others a pro-survival/oncogenic function[12, 29, 32-34, 36]. Based on our data, we suspect that MARK- and 14-3-3-mediated suppression of TNK1 may be a point of deregulation in cancer to 'turn on' TNK1. One example is the Hodgkin lymphoma cell line L540, in which a paracentric inversion has generated a truncated TNK1 that lacks the 14-3-3 binding site. As our model would predict (Supplemental. Figure 2-5B), this truncated TNK1 is active [32], drives the growth of L540 cells (Figure 2-6D), and is oncogenic in the Ba/F3 system (Supplemental. Figure 2-5A), all of which is consistent with our data. Our efforts to determine whether this truncation is frequent in cancer have been challenging—the inversion is too small to be effectively probed by Fluorescence in situ hybridization (FISH), so the answer will likely be found in unfiltered data from genome sequencing. Our model also suggests that cancers deficient in LKB1 may have higher levels of active TNK1 (via inactivation of MARKs). We propose that these observations help guide future work to evaluate TNK1 as a therapeutic target in specific cancer settings.

In summary, these data provide a new mechanism of regulation for an understudied tyrosine kinase and a template to target its activity in cancer. The involvement of a UBA domain in this

mechanism underscores the need for a better understanding of PTM-binding domains in kinase biology. Other PTM-binding domains, including bromodomains, chromodomains, as well as other types of ubiquitin-binding domains (e.g., zinc finger), likely play underappreciated roles in helping kinases integrate signals from complex signaling networks[40, 90]. In addition, the relationship between 14-3-3 and TNK1 sheds new light on 14-3-3-mediated regulation of kinases. Recent mechanistic studies on 14-3-3-mediated regulation of BRAF also help expand the paradigm of 14-3-3-kinase relationships [63, 64]. It is likely that other kinases are similarly regulated by 14-3-3, but their discovery will require deeper LC-MS/MS probing of the 14-3-3 interactome.

2.6. Acknowledgements

We thank the Fritz B. Burns Foundation for student and postdoctoral salary support to LJL, KK, KLP and critical instrumentation. We acknowledge Duke University School of Medicine for the use of the Proteomics and Metabolomics Shared Resource, which provided TiO_2 and pY proteomics data. We acknowledge the Preclinical Research Resource (PRR) at the Huntsman Cancer Institute, which provided mice, surgical procedures, IVIS imaging and histology service. We thank Tony Pomicter and members of Michael Deininger's lab for key reagents and guidance on the project. We thank Drs. Rafael Casellas, Jens Kalchschmidt, as well as all members of the Casellas, Andersen and Huang labs for constructive discussion and scientific input. We thank Drs. Alana Welm, Grant Dewson, Mark van Delft, Denis Tvorgorov, Isabelle Lucet and David Komander for technical assistance and insights into kinase/ubiquitin biology. We thank the Simmons Center for Cancer Research, Roland K. Robins and the BYU College of Physical and Mathematical Sciences for graduate fellowships to TYC; and graduate studies for a HIDRA fellowship to CME. JEM is supported by an American Society of Hematology Scholar Award, American Cancer Society Research Scholar Grant RSG-19-184-01, a Lamfrom Laureate Award,

and R00 CA190605 from the National Cancer Institute. JLA is supported by an American Cancer Society Research Scholar Grant (133550-RSG-19-006-01-CCG) (2019-current) and a National Cancer Institute/National Institutes of Health grant (2R15CA202618-02).

2.7. Supplementary Figures

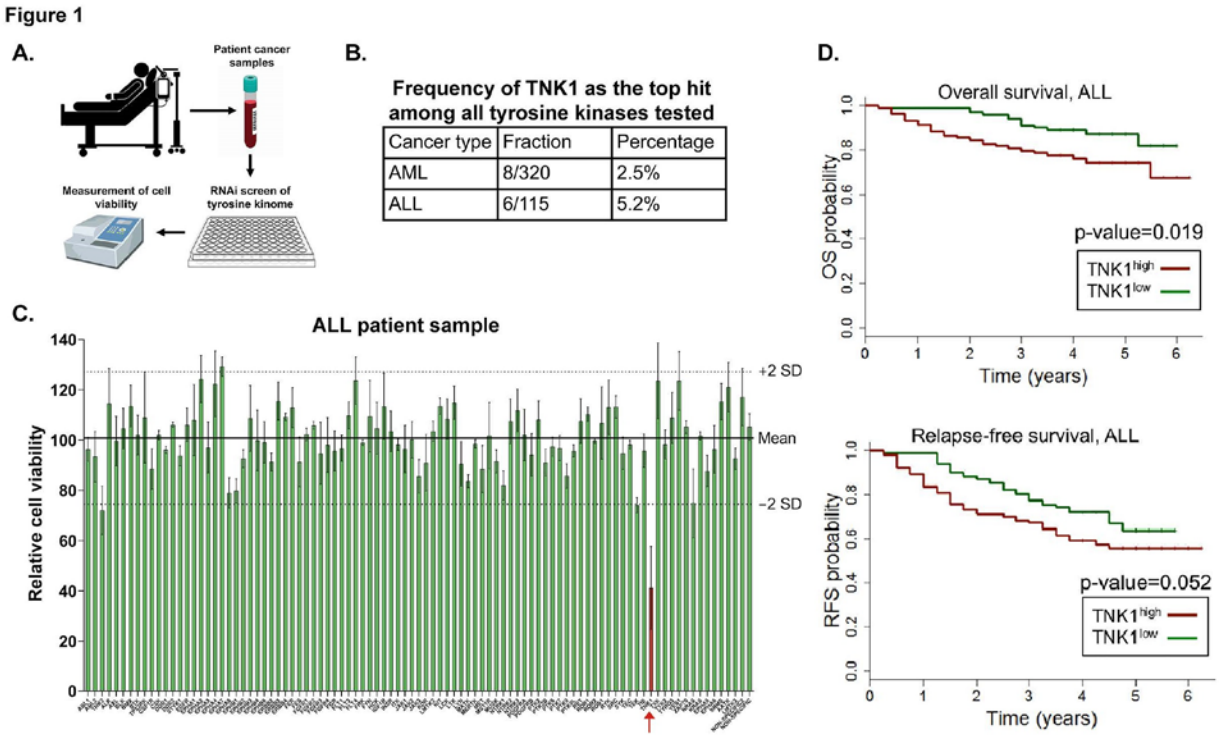

Supplementary Figure 2-1. RNAi screening of tyrosine kinases across human hematological cancer patient samples reveals a dependency on the non-receptor tyrosine kinase TNK1.

(A) Schematic diagram of RNAi screening of tyrosine kinases across 435 hematological cancer samples from human patients. Samples were subjected to an RNAi screen of human tyrosine kinases, followed by measurement of cell viability.

(B) Frequency of TNK1 as the top hit (defined as the tyrosine kinase that, when depleted, has the largest negative impact on cell survival in a given sample) from the RNAi screening of tyrosine kinases in AML and ALL. Hit threshold is defined as 2 standard deviations below the mean viability.

(C) A representative viability assay from an ALL patient sample showing TNK1 as the top hit (red bar).

(D) Kaplan Meier graphs showing correlations between TNK1 mRNA levels and overall survival and relapse-free survival in ALL patients (COG P9906 B-ALL trial, n=207). The data are derived from gene expression microarray data of 207 pre-B ALL patients in the Children's Oncology Group (COG) Clinical Trial P9906. Patient survival data were obtained from the National Cancer Institute TARGET Data Matrix (http://targetnci.nih.gov/dataMatrix/TARGET_DataMatrix.html).

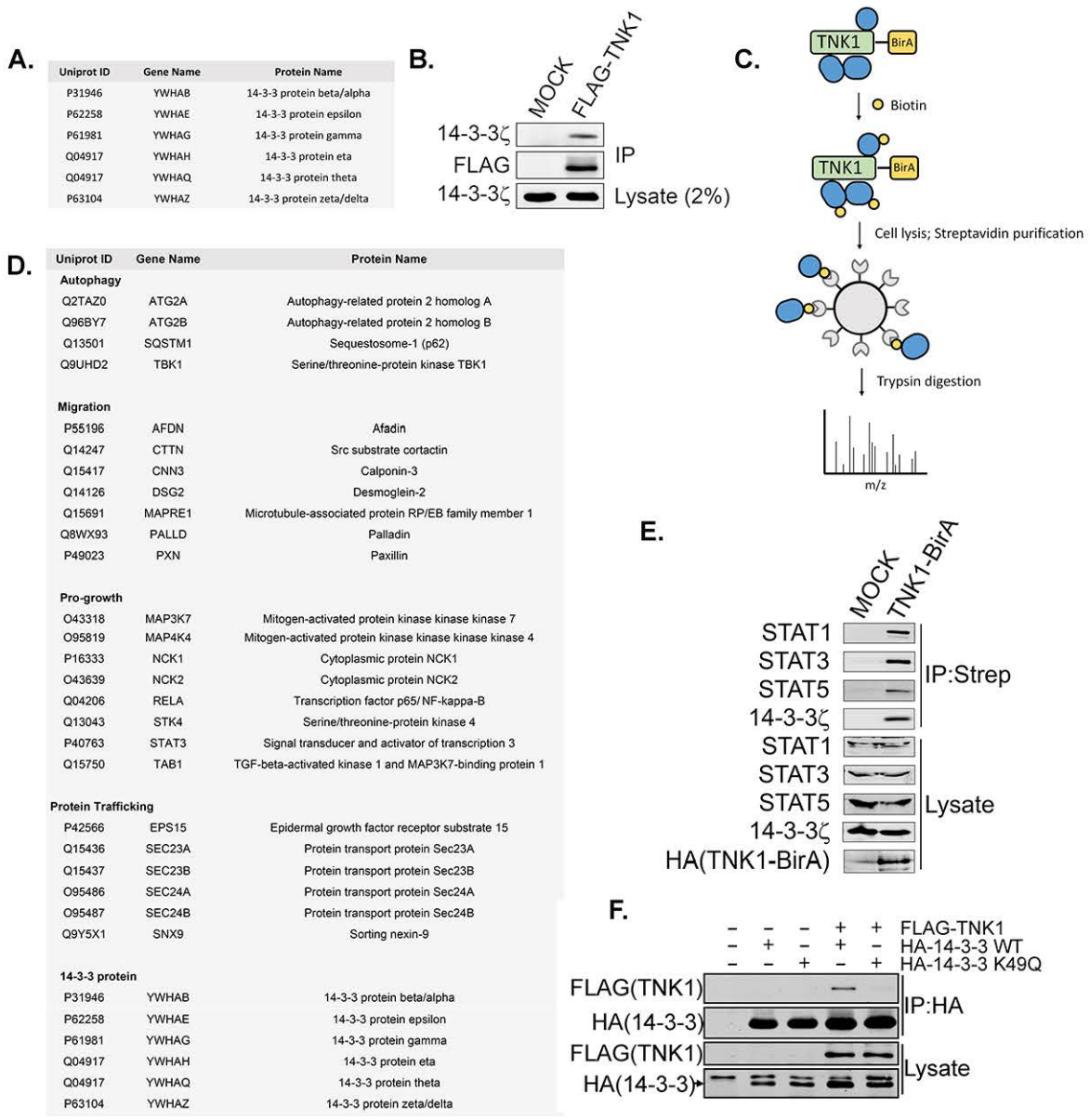

Uniprot ID	Gene Name	Protein Name
P31946	YWHAB	14-3-3 protein beta/alpha
P62258	YWHAE	14-3-3 protein epsilon
P61981	YWHAG	14-3-3 protein gamma
Q04917	YWHAH	14-3-3 protein eta
Q04917	YWHAQ	14-3-3 protein theta
P63104	YWHAZ	14-3-3 protein zeta/delta

Uniprot ID	Gene Name	Protein Name
Autophagy		
Q2TAZ0	ATG2A	Autophagy-related protein 2 homolog A
Q96BY7	ATG2B	Autophagy-related protein 2 homolog B
Q13501	SQSTM1	Sequestosome-1 (p62)
Q9UHD2	TBK1	Serine/threonine-protein kinase TBK1
Migration		
P55196	AFDN	Afadin
Q14247	CTTN	Src substrate cortactin
Q15417	CNN3	Calponin-3
Q14126	DSG2	Desmoglein-2
Q15691	MAPRE1	Microtubule-associated protein RP/EB family member 1
Q8WX93	PALLD	Palladin
P49023	PXN	Paxillin
Pro-growth		
O43318	MAP3K7	Mitogen-activated protein kinase kinase kinase 7
O95819	MAP4K4	Mitogen-activated protein kinase kinase kinase kinase 4
P16333	NCK1	Cytoplasmic protein NCK1
O43639	NCK2	Cytoplasmic protein NCK2
Q04206	RELA	Transcription factor p65/ NF-kappa-B
Q13043	STK4	Serine/threonine-protein kinase 4
P40763	STAT3	Signal transducer and activator of transcription 3
Q15750	TAB1	TGF-beta-activated kinase 1 and MAP3K7-binding protein 1
Protein Trafficking		
P42566	EPS15	Epidermal growth factor receptor substrate 15
Q15436	SEC23A	Protein transport protein Sec23A
Q15437	SEC23B	Protein transport protein Sec23B
O95486	SEC24A	Protein transport protein Sec24A
O95487	SEC24B	Protein transport protein Sec24B
Q9Y5X1	SNX9	Sorting nexin-9
14-3-3 protein		
P31946	YWHAB	14-3-3 protein beta/alpha
P62258	YWHAE	14-3-3 protein epsilon
P61981	YWHAG	14-3-3 protein gamma
Q04917	YWHAH	14-3-3 protein eta
Q04917	YWHAQ	14-3-3 protein theta
P63104	YWHAZ	14-3-3 protein zeta/delta

Supplementary Figure 2-2. Co-IP and BioID proteomics identify 14-3-3 as an interacting partner of TNK1.

(A) FLAG-TNK1 was expressed in HEK-293T cells, immunoprecipitated on FLAG resin, followed by elution of interacting partners and analysis by LC-MS/MS.
(B) FLAG-TNK1 was immunoprecipitated as in panel A, then subject to immunoblot with indicated antibodies.
(C) Schematic of TNK1 BioID.
(D) TNK1-BirA was expressed in HEK-293T cells supplemented with biotin, followed by isolation of biotinylated proteins on streptavidin resin and analysis by LC-MS/MS.
(E) Streptavidin pulldowns from panel D were immunoblotted with indicated antibodies.
(F) HA-14-3-3 (WT or K49Q) was co-expressed with FLAG-TNK1 in HEK-293T cells, followed by immunoprecipitation of HA-14-3-3 and immunoblotting with indicated antibodies.

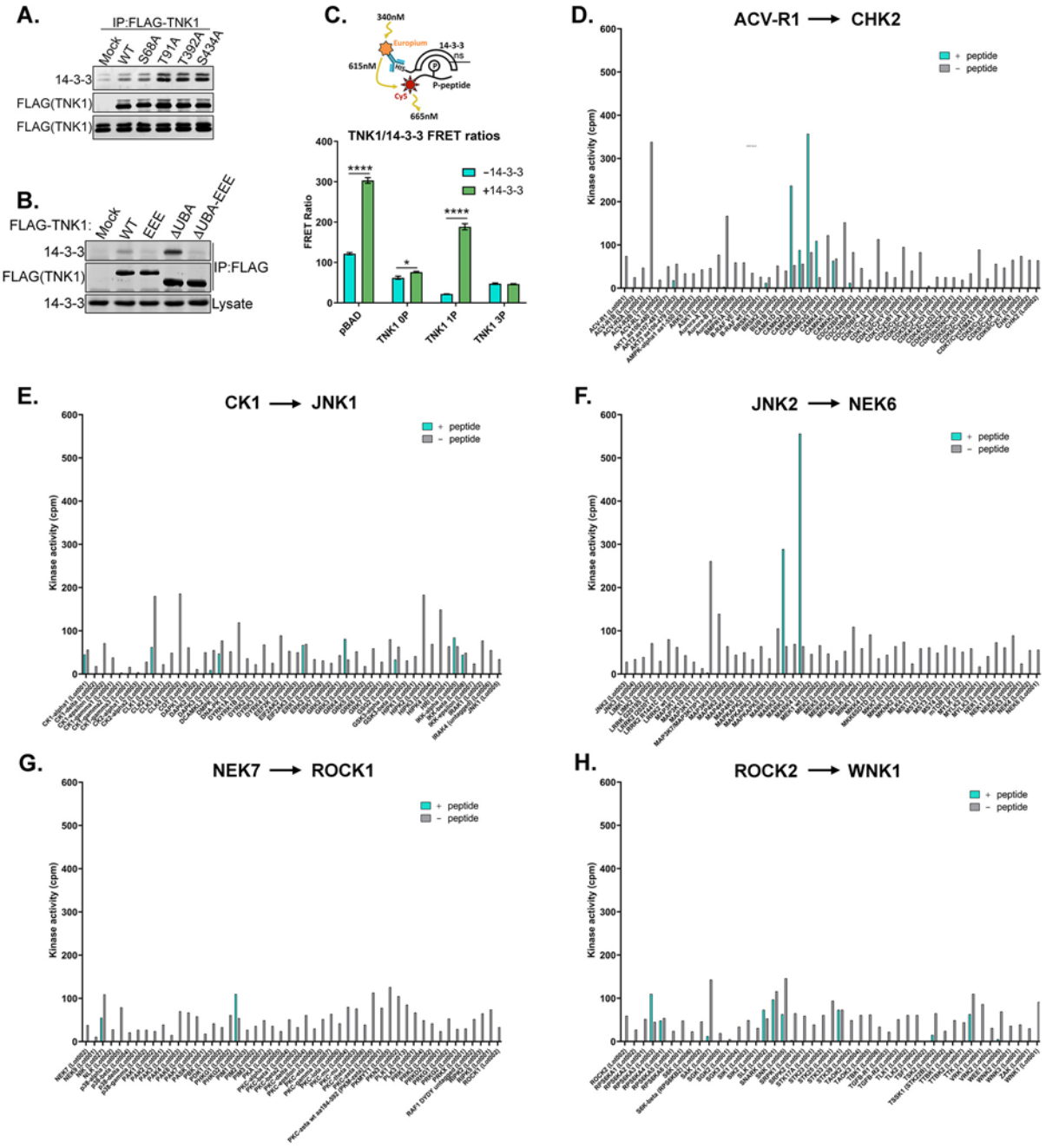

Supplementary Figure 2-3. A MARK-mediated 14-3-3 binding motif that encompasses S502 of TNK1.

(A) WT or S/T-to-A mutants of FLAG-TNK1 were expressed in HEK-293T cells, immunoprecipitated on FLAG resin and immunoblotted with indicated antibodies.

(B) WT or S-to-E triple mutant (S500E/S502E/S505E) of FLAG-TNK1 were expressed in HEK-293T cells, immunoprecipitated on FLAG resin and immunoblotted with indicated antibodies.

(C) Schematic representation of FRET assay monitoring interaction between 14-3-3 and TNK1 peptide (amino acid 488-511). TNK1 0P peptide has no phosphorylation. TNK1 1P peptide is

mono-phosphorylated at S502. TNK1 3P peptide contains phosphorylations on S500, S502 and S505. Graph shows average FRET ratios with error bars representing SEM.

(D)-(H) A N-terminally biotinylated 13-mer TNK1 peptide encompassing S502 was incubated in a streptavidin-coated FlashPlateTM and subjected to a radiometric kinase assay with 245 individual S/T protein kinases. To account for signal from kinase autophosphorylation, each assay (+ peptide) was normalized to a control with the kinase but no peptide.

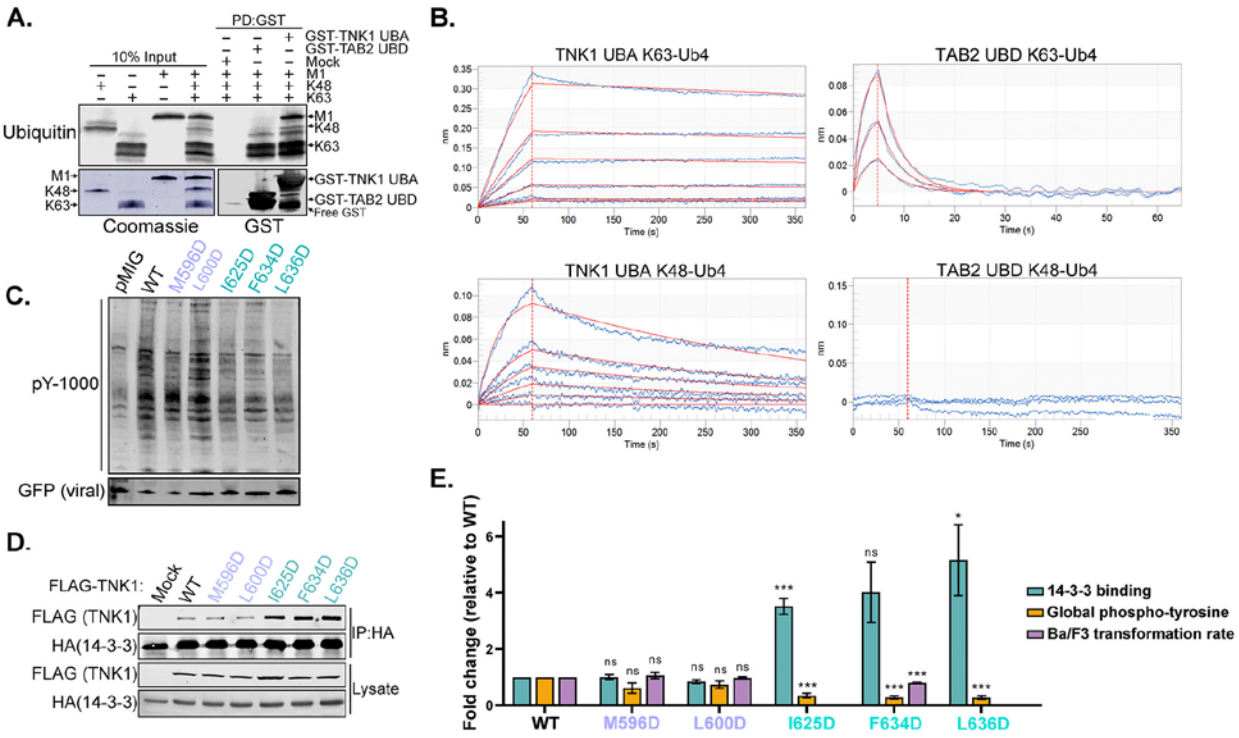

Supplementary Figure 2-4. TNK1 UBA domain binds poly-ubiquitin with a high affinity and is essential for TNK1 activity.

(A) Recombinant GST-TNK1-UBA or GST-TAB2-UBD were incubated with the combined indicated tetra-ubiquitin for a competitive pull-down experiment at 4ºC for 2 hours. GST tagged proteins were captured on glutathione resin and immunoblotted for GST and ubiquitin. A 10% input of tetra-ubiquitin for each linkage type was also visualized by Coomassie staining of SDS-PAGE gel to indicate differences in gel migration of the linkages.

(B) Bio-layer interferometry (BLI) was performed to characterize the binding between TNK1-UBA/TAB2-UBD and tetra-ubiquitin. Binding kinetics were obtained from fitting processed data to a 1:1 binding model. Graphs show representative BLI sensorgram and fit for TNK1-UBA/TAB2-UBD and tetra-ubiquitin.

(C) Mock- or TNK1-expressing Ba/F3 cells from Figure 3 panel G were immunoblotted for global phospho-tyrosine as an indicator of TNK1 activity. Cells were also immunoblotted for GFP (expressed from the TNK1-expressing retrovirus) as a loading control.

(D) HEK293T cells stably expressing HA-14-3-3ζwere transfected with WT FLAG-TNK1, followed by immunoprecipitation on HA resin and immunoblotting for FLAG.

(E) Quantitation of Figure 3 panel G in the form of transformation rate, as well as (C) and (D) from multiple replicates, shown with signals normalized to WT TNK1. Error bars represent SEM.

A.

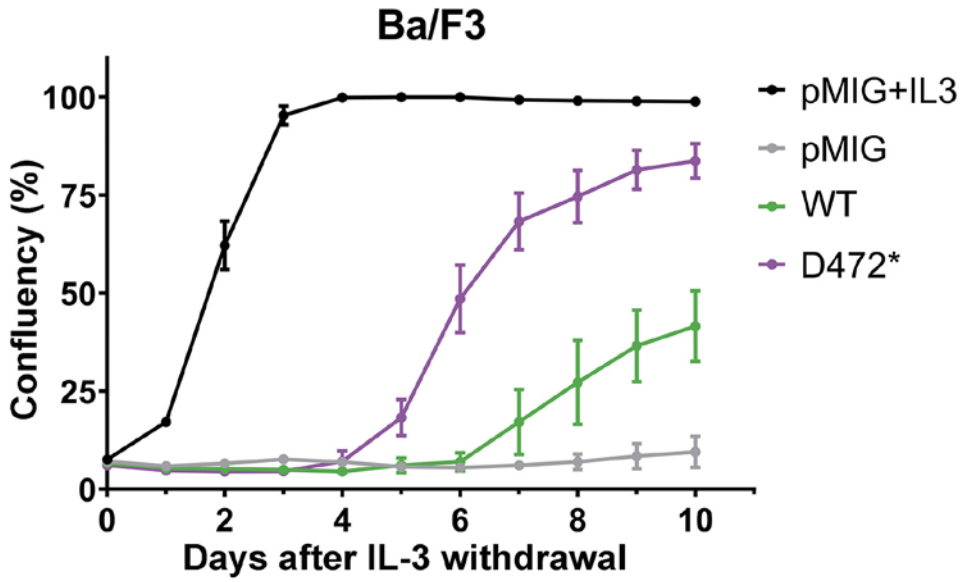

B.

Status	Effect	Activity
WT 	NA	- +
AAA 	No 14-3-3 binding	+ + +
ΔUBA 	No ubiquitin binding	- -
ΔUBA-AAA 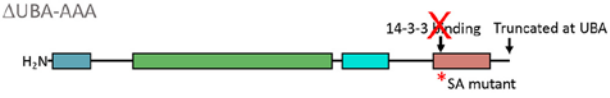	No 14-3-3 binding No ubiquitin binding	- + +
Paracentric inversion, HL line 	No 14-3-3 binding No ubiquitin binding	- + +

Supplementary Figure 2-5. A mutant of TNK1, generated by paracentric inversion in a Hodgkin lymphoma cell line, drives growth factor-independent proliferation.

(A) Ba/F3 cells were transduced with either pMIG-empty vector, WT TNK1 or the D472* TNK1 (to mimic the naturally occurring mutation in L540 cells) were analyzed for IL-3 independent growth as in figure 3G.

(B) A table showing the effect of various mutations on TNK1 kinase activity.

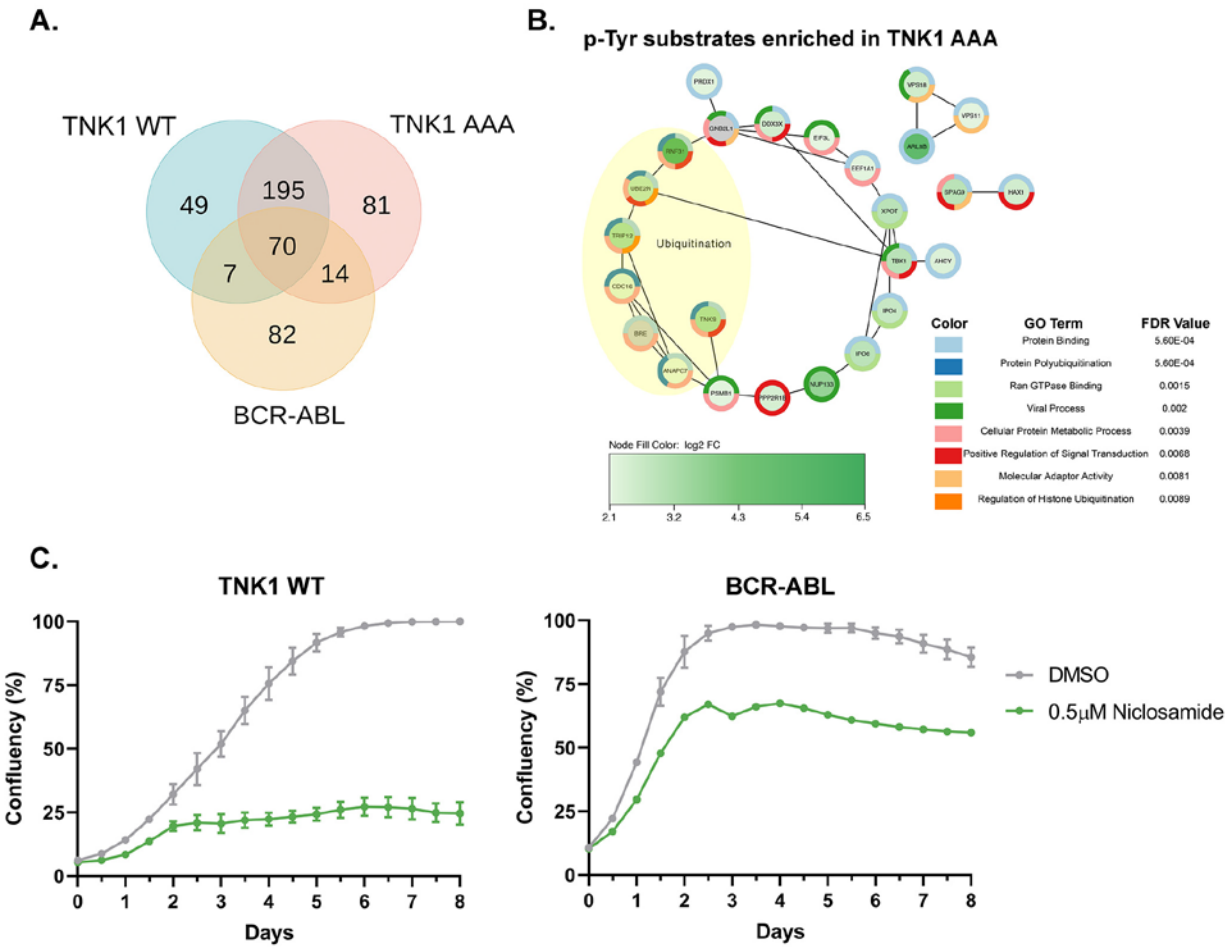

Supplementary Figure 2-6. Bioinformatics evaluation of putative TNK1 substrates.

(A) Venn diagram of unique protein from each category. Included proteins are at least 2-fold higher in signal comparative to background (MOCK) and have a p-value lower than 0.05.

(B) Phospho-tyrosine substrates that were significant and displayed a fold change of two or greater (relative to control) in TNK1-AAA alone were subjugated to STRING DB network analysis and visualized in Cytoscape. Node color represents magnitude of fold change. A ubiquitin-related subset of interactors (highlighted) was selected using GO-terms and manual curation.

(C) TNK1-WT- driven Ba/F3 cells and BCR-ABL-driven Ba/F3 cells were treated with vehicle (DMSO) or 0.5 μM Niclosamide for 72 indicated time. Cell confluency was measured using IncuCyte imaging system.

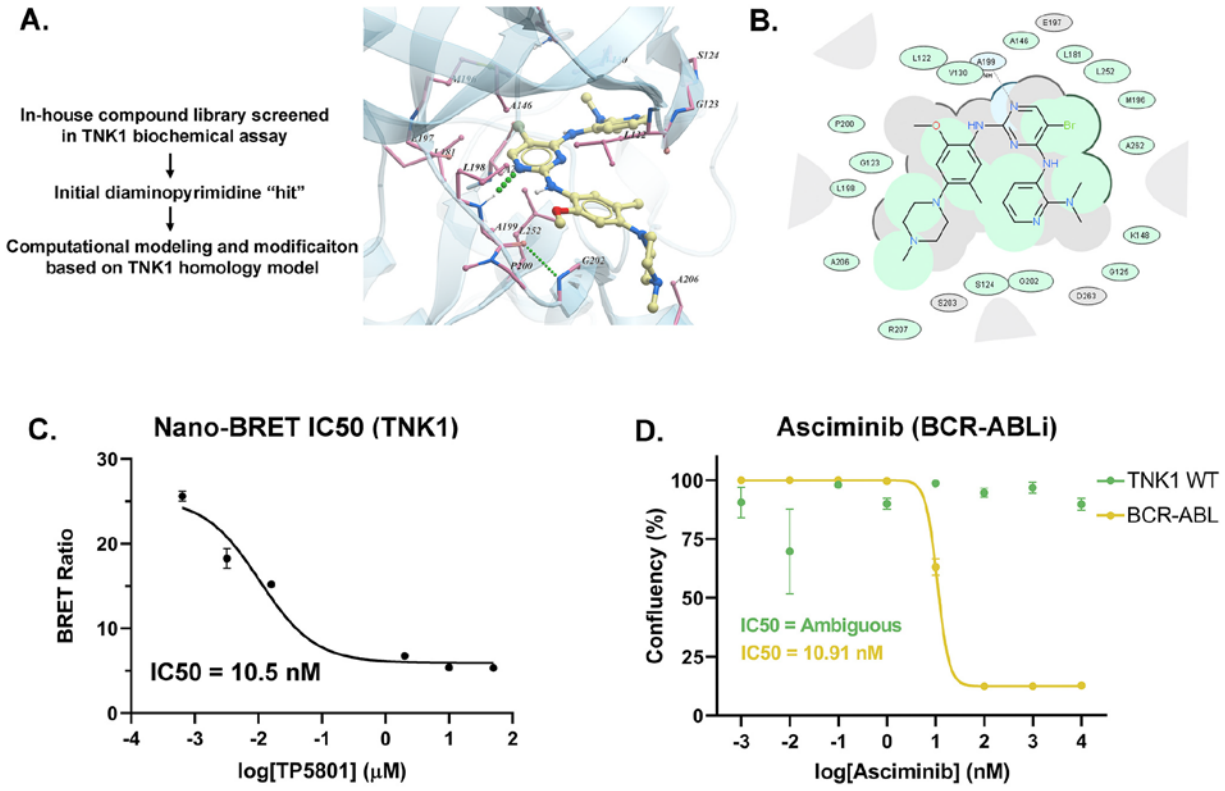

Supplementary Figure 2-7. The development of a potent TNK1 inhibitor, TP-5801.

(A) Left panel shows a schematic outline of the development of TP-5801. Right panel shows the TP-801 docking pose in the TNK1 active site homology model.
(B) Schematic diagam of TP-5801 docking pose in the TNK1 active site homology model.
(C) Diagram of TP-5801 nano-BRET IC50.
(D) IC50 graph of TNK1-WT driven Ba/F3 cells or BCR-ABL-driven Ba/F3 cells treated with Asciminib (1pM to 10mM) for 72 hours. Cell confluency was measured using IncuCyte imaging system.

3. Future Directions and Summary

3.1. Role of TNK1 UBA in regulating kinase activity

Our data reveal the first regulatory mechanism of the poorly understood tyrosine kinase TNK1 by 14-3-3 binding and ubiquitin-binding property of its UBA domain. While it seems clear that 14-3-3 binding on TNK1 controls its localization/clustering, the role the UBA plays in kinase activation requires further investigation. To our knowledge, TNK1 is the first example of a kinase possessing a functional ubiquitin-binding UBA domain, which TNK1 relies on for full kinase activation. This concept raises interesting questions for future studies.

First, is ubiquitin binding alone sufficient to activate TNK1? From our data, mutations that interrupt ubiquitin binding reduced TNK1 kinase activity. This observation suggests that ubiquitin binding is an essential part of the TNK1 mechanism of activation. Second, since UBA domains are often found in proteins involved in degradation pathways, could TNK1 play a role in proteasomal degradation or autophagy? p62/SQSTM1 is an autophagy receptor, which also has a functional UBA domain at its C-terminus[91, 92]. With the UBA domain, p62 binds and loads ubiquitinated cargo to the autophagosome for degradation. From our BioID data, we found that TNK1 interacts with multiple autophagy-related proteins, including p62/SQSTM1, ATG2A/B and TBK1. Our confocal data confirms that TNK1 co-localizes with p62/SQSTM1 (figure 3-1). We also found that TNK1 interacts with all three forms of the autophagy marker light chain 3 (LC3) (data not shown). However, the question of whether TNK1 plays a role in autophagy or simply is degraded via autophagy still requires further investigation. Third, is the UBA domain of ACK1, the only other human kinase in the ACK family, also functional and does it play a role in kinase regulation? There is no still study validating whether the ACK1 UBA can bind to ubiquitin. However, a mutation within the UBA domain of ACK1 led to increased cancer cell proliferation

and migration[45]. The mechanism of how the mutation affects ACK1 kinase activity and its UBA will be an important future direction.

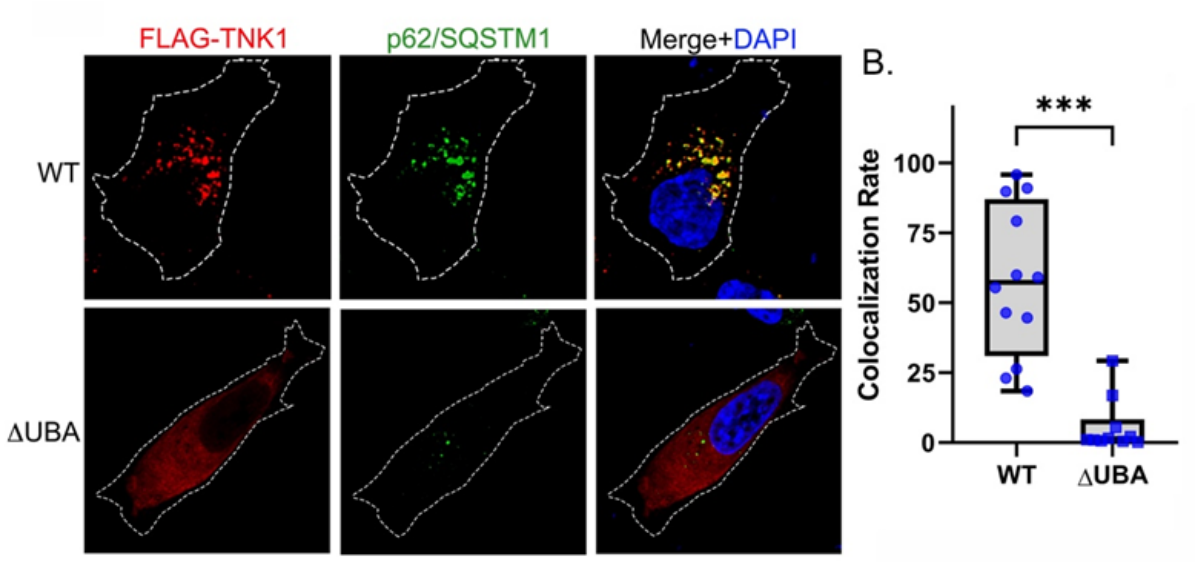

Figure 3-1 TNK1 UBA domain is required for co-localization with p62/SQSTM1.

(A) HEK-293A cells expressing FLAG-TNK1 (WT or ΔUBA) were analyzed by confocal imaging for FLAG-TNK1 and p62/SQSTM1 localization.
(B) FLAG-TNK1 and p62/SQSTM1 co-localization was analyzed using Leica 3D analysis.

Within the TNK1 UBA domain, there is a prominent tyrosine phosphorylation. Indeed, it is the most frequently identified tyrosine phosphorylation across the entire sequence of TNK1. We found that a phospho-defective mutation at this site (Y661F) slightly reduced 14-3-3 binding on TNK1, while a phospho-mimicking mutation (Y661E) increased 14-3-3 binding on TNK1 (figure 3-2). Given the importance of the UBA in TNK1 activity, I posit that phosphorylation of Y661 could be an important regulatory mechanism for TNK1. However, we still do not know the precise function of Y661 phosphorylation (most importantly, its effect on ubiquitin binding), nor the kinase that mediates this phosphorylation (these studies are currently underway)

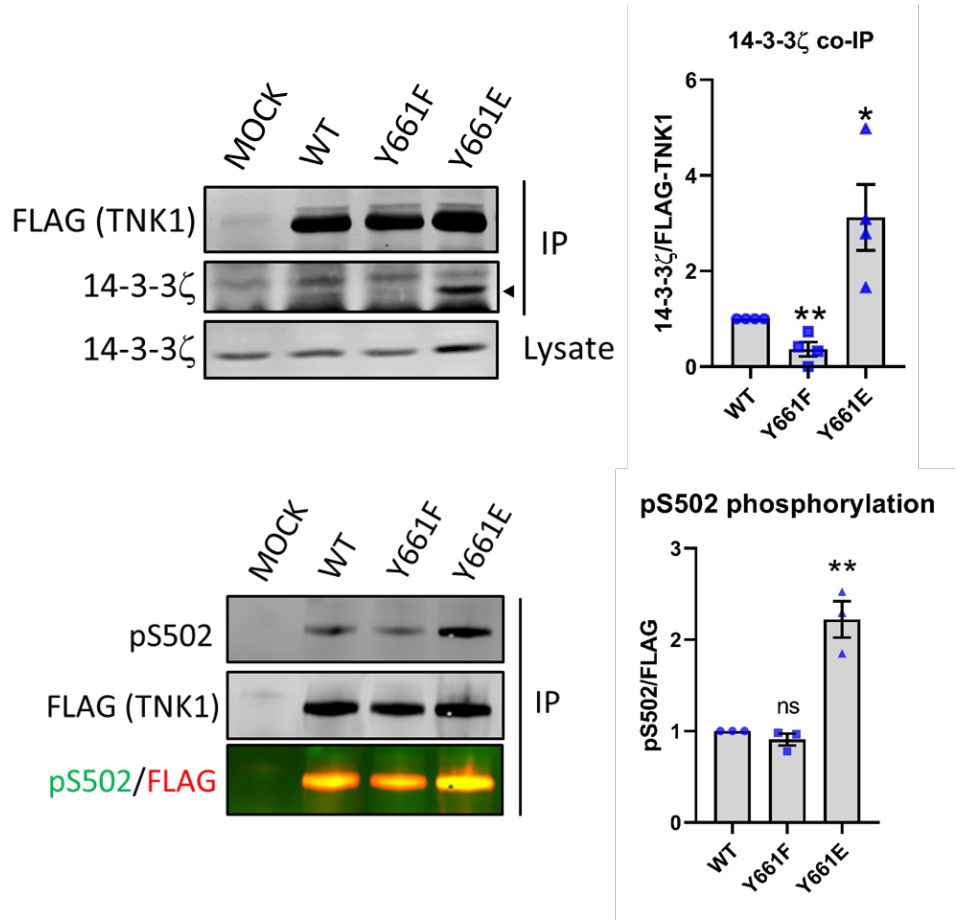

Figure 3-2 Phospho-mimicking mutation at Y661 increases phosphorylation at S502 and 14-3-3 binding. WT and mutant FLAG-TNK1 were immunoprecipitated from HEK-293T cells and immunoblotted for 14-3-3 binding (upper) and TNK1 phosphorylation at S502 (lower). Graphs show quantitation of infrared signal from multiple replicates with signals normalized to WT. Error bars represent SEM.

3.2. Oligomerization

NRTK activity often requires dimerization/oligomerization. ACK1 requires its N-terminal SAM domain for dimerization and activation. The ACK1 SAM domain is also required for membrane association[4]. (Interestingly, mutations within the SAM domain, R34L and R99Q, activate ACK1 by an unknown mechanism.[11]) Like ACK1, TNK1 also possesses an N-terminal SAM domain. We have posited that interactions between the TNK1 UBA and ubiquitin may

facilitate TNK1 oligomerization by a mechanism of "induced proximity". However, the requirement for oligomerization in TNK1 activation and the role of the UBA in the process, is currently known.

3.3. Migration

We have shown, via Bio-ID proteomics, that TNK1 interacts with multiple migration-related proteins (sup. figure 2-2). These data made us question whether TNK1 may be involved in promoting cell motility. To test this idea, we demonstrated that TNK1 KO cells show limited movement comparing to the WT cell and it is demonstrated in different cell lines (figure 3-3). These data suggest that TNK1 promotes cancer cell motility.

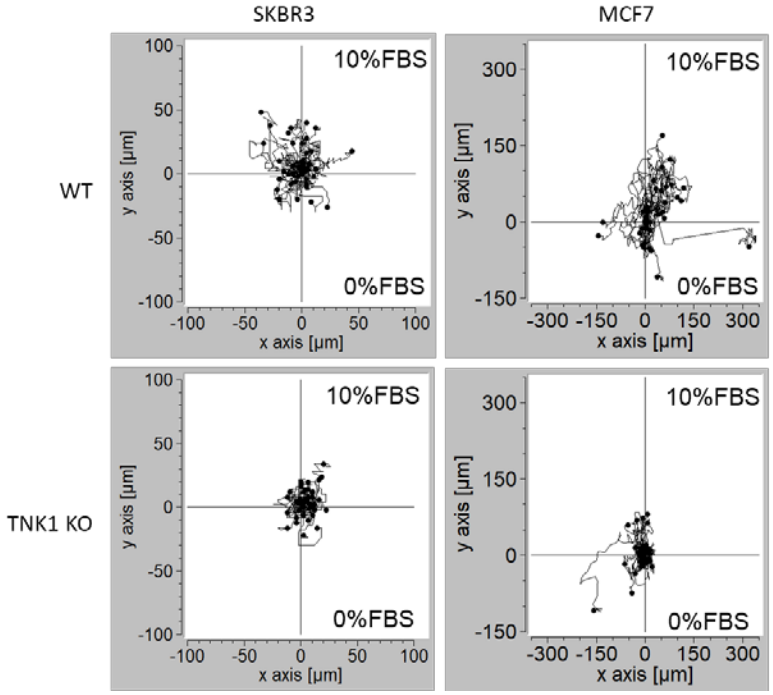

Figure 3-3 TNK1 KO restrains cells migration. SKBR3 and MCF7 CRISPR/Cas9 TNK1 KO and parental cell lines were analyzed for motility in a CellASCICS chamber. Cells were tracked every 10 minutes for 12 hours. The path of each cell and distance traveled is shown by each line in graphs on left.

3.4. Summary

In conclusion, our data uncover the first mechanism of TNK1 regulation, including the first example of a functional UBA domain on a kinase. We have also discovered a lead compound for development of a TNK1-targeted therapeutic. However, there is still much work to be done to understand the general function of TNK1 in human biology and additional details regarding TNK1 regulation. The unpublished preliminary data shown in this chapter demonstrate a few of the important future directions for this project, including 1) the interacting partners of TNK1; 2) additional regulatory modifications on TNK1; 3) the normal function/role of TNK1 in cells. In addition, it will be important to thoroughly characterize the role of ubiquitin binding in TNK1 activation and function.

4. Reference

[1] Bergethon, K., Shaw, A. T., Ou, S. H., Katayama, R., Lovly, C. M., McDonald, N. T., Massion, P. P., Siwak-Tapp, C., Gonzalez, A., Fang, R., Mark, E. J., Batten, J. M., Chen, H., Wilner, K. D., Kwak, E. L., Clark, J. W., Carbone, D. P., Ji, H., Engelman, J. A., Mino-Kenudson, M., Pao, W., and Iafrate, A. J. (2012) ROS1 rearrangements define a unique molecular class of lung cancers, *J Clin Oncol 30*, 863-870.

[2] Creancier, L., Vandenberghe, I., Gomes, B., Dejean, C., Blanchet, J. C., Meilleroux, J., Guimbaud, R., Selves, J., and Kruczynski, A. (2015) Chromosomal rearrangements involving the NTRK1 gene in colorectal carcinoma, *Cancer Lett 365*, 107-111.

[3] Soda, M., Choi, Y. L., Enomoto, M., Takada, S., Yamashita, Y., Ishikawa, S., Fujiwara, S., Watanabe, H., Kurashina, K., Hatanaka, H., Bando, M., Ohno, S., Ishikawa, Y., Aburatani, H., Niki, T., Sohara, Y., Sugiyama, Y., and Mano, H. (2007) Identification of the transforming EML4-ALK fusion gene in non-small-cell lung cancer, *Nature 448*, 561-566.

[4] Prieto-Echague, V., Gucwa, A., Brown, D. A., and Miller, W. T. (2010) Regulation of Ack1 localization and activity by the amino-terminal SAM domain, *BMC Biochem 11*, 42.

[5] Gajiwala, K. S., Maegley, K., Ferre, R., He, Y. A., and Yu, X. (2013) Ack1: activation and regulation by allostery, *PLoS One 8*, e53994.

[6] Prieto-Echague, V., and Miller, W. T. (2011) Regulation of ack-family nonreceptor tyrosine kinases, *J Signal Transduct 2011*, 742372.

[7] Galisteo, M. L., Yang, Y., Urena, J., and Schlessinger, J. (2006) Activation of the nonreceptor protein tyrosine kinase Ack by multiple extracellular stimuli, *Proc Natl Acad Sci U S A 103*, 9796-9801.

[8] Chan, W., Sit, S. T., and Manser, E. (2011) The Cdc42-associated kinase ACK1 is not autoinhibited but requires Src for activation, *Biochem J 435*, 355-364.

[9] Grovdal, L. M., Johannessen, L. E., Rodland, M. S., Madshus, I. H., and Stang, E. (2008) Dysregulation of Ack1 inhibits down-regulation of the EGF receptor, *Exp Cell Res 314*, 1292-1300.

[10] Teo, M., Tan, L., Lim, L., and Manser, E. (2001) The tyrosine kinase ACK1 associates with clathrin-coated vesicles through a binding motif shared by arrestin and other adaptors, *J Biol Chem 276*, 18392-18398.

[11] Prieto-Echague, V., Gucwa, A., Craddock, B. P., Brown, D. A., and Miller, W. T. (2010) Cancer-associated mutations activate the nonreceptor tyrosine kinase Ack1, *J Biol Chem 285*, 10605-10615.

[12] Azoitei, N., Brey, A., Busch, T., Fulda, S., Adler, G., and Seufferlein, T. (2007) Thirty-eight-negative kinase 1 (TNK1) facilitates TNFalpha-induced apoptosis by blocking NF-kappaB activation, *Oncogene 26*, 6536-6545.

[13] Armacki, M., Trugenberger, A. K., Ellwanger, A. K., Eiseler, T., Schwerdt, C., Bettac, L., Langgartner, D., Azoitei, N., Halbgebauer, R., Gross, R., Barth, T., Lechel, A., Walter, B. M., Kraus, J. M., Wiegreffe, C., Grimm, J., Scheffold, A., Schneider, M. R., Peuker, K., Zeissig, S., Britsch, S., Rose-John, S., Vettorazzi, S., Wolf, E., Tannapfel, A., Steinestel, K., Reber, S. O., Walther, P., Kestler, H. A., Radermacher, P., Barth, T. F., Huber-Lang, M., Kleger, A., and Seufferlein, T. (2018) Thirty-eight-negative kinase 1 mediates trauma-induced intestinal injury and multi-organ failure, *J Clin Invest 128*, 5056-5072.

[14] Jones, S., Cunningham, D. L., Rappoport, J. Z., and Heath, J. K. (2014) The non-receptor tyrosine kinase Ack1 regulates the fate of activated EGFR by inducing trafficking to the p62/NBR1 pre-autophagosome, *J Cell Sci 127*, 994-1006.

[15] Shen, F., Lin, Q., Gu, Y., Childress, C., and Yang, W. (2007) Activated Cdc42-associated kinase 1 is a component of EGF receptor signaling complex and regulates EGF receptor degradation, *Mol Biol Cell 18*, 732-742.

[16] Zhang, J., Chen, T., Mao, Q., Lin, J., Jia, J., Li, S., Xiong, W., Lin, Y., Liu, Z., Liu, X., Zhao, H., Wang, G., Zheng, D., Qiu, S., and Ge, J. (2015) PDGFR-beta-activated ACK1-AKT signaling promotes glioma tumorigenesis, *Int J Cancer 136*, 1769-1780.
[17] Modzelewska, K., Newman, L. P., Desai, R., and Keely, P. J. (2006) Ack1 mediates Cdc42-dependent cell migration and signaling to p130Cas, *J Biol Chem 281*, 37527-37535.
[18] Mahajan, K., Malla, P., Lawrence, H. R., Chen, Z., Kumar-Sinha, C., Malik, R., Shukla, S., Kim, J., Coppola, D., Lawrence, N. J., and Mahajan, N. P. (2017) ACK1/TNK2 Regulates Histone H4 Tyr88-phosphorylation and AR Gene Expression in Castration-Resistant Prostate Cancer, *Cancer Cell 31*, 790-803 e798.
[19] Mahajan, N. P., Liu, Y., Majumder, S., Warren, M. R., Parker, C. E., Mohler, J. L., Earp, H. S., and Whang, Y. E. (2007) Activated Cdc42-associated kinase Ack1 promotes prostate cancer progression via androgen receptor tyrosine phosphorylation, *Proc Natl Acad Sci U S A 104*, 8438-8443.
[20] Jenkins, C., Luty, S. B., Maxson, J. E., Eide, C. A., Abel, M. L., Togiai, C., Nemecek, E. R., Bottomly, D., McWeeney, S. K., Wilmot, B., Loriaux, M., Chang, B. H., and Tyner, J. W. (2018) Synthetic lethality of TNK2 inhibition in PTPN11-mutant leukemia, *Sci Signal 11*.
[21] Mahajan, N. P., Coppola, D., Kim, J., Lawrence, H. R., Lawrence, N. J., and Mahajan, K. (2018) Blockade of ACK1/TNK2 To Squelch the Survival of Prostate Cancer Stem-like Cells, *Sci Rep 8*, 1954.
[22] Mahajan, N. P., Whang, Y. E., Mohler, J. L., and Earp, H. S. (2005) Activated tyrosine kinase Ack1 promotes prostate tumorigenesis: role of Ack1 in polyubiquitination of tumor suppressor Wwox, *Cancer Res 65*, 10514-10523.
[23] Maxson, J. E., Abel, M. L., Wang, J., Deng, X., Reckel, S., Luty, S. B., Sun, H., Gorenstein, J., Hughes, S. B., Bottomly, D., Wilmot, B., McWeeney, S. K., Radich, J., Hantschel, O., Middleton, R. E., Gray, N. S., Druker, B. J., and Tyner, J. W. (2016) Identification and Characterization of Tyrosine Kinase Nonreceptor 2 Mutations in Leukemia through Integration of Kinase Inhibitor Screening and Genomic Analysis, *Cancer Res 76*, 127-138.
[24] Maxson, J. E., Gotlib, J., Pollyea, D. A., Fleischman, A. G., Agarwal, A., Eide, C. A., Bottomly, D., Wilmot, B., McWeeney, S. K., Tognon, C. E., Pond, J. B., Collins, R. H., Goueli, B., Oh, S. T., Deininger, M. W., Chang, B. H., Loriaux, M. M., Druker, B. J., and Tyner, J. W. (2013) Oncogenic CSF3R mutations in chronic neutrophilic leukemia and atypical CML, *N Engl J Med 368*, 1781-1790.
[25] Wu, X., Zahari, M. S., Renuse, S., Kelkar, D. S., Barbhuiya, M. A., Rojas, P. L., Stearns, V., Gabrielson, E., Malla, P., Sukumar, S., Mahajan, N. P., and Pandey, A. (2017) The non-receptor tyrosine kinase TNK2/ACK1 is a novel therapeutic target in triple negative breast cancer, *Oncotarget 8*, 2971-2983.
[26] Fox, M., Crafter, C., and Owen, D. (2019) The non-receptor tyrosine kinase ACK: regulatory mechanisms, signalling pathways and opportunities for attACKing cancer, *Biochem Soc Trans 47*, 1715-1731.
[27] Hoehn, G. T., Stokland, T., Amin, S., Ramirez, M., Hawkins, A. L., Griffin, C. A., Small, D., and Civin, C. I. (1996) Tnk1: a novel intracellular tyrosine kinase gene isolated from human umbilical cord blood CD34+/Lin-/CD38- stem/progenitor cells, *Oncogene 12*, 903-913.
[28] Felschow, D. M., Civin, C. I., and Hoehn, G. T. (2000) Characterization of the tyrosine kinase Tnk1 and its binding with phospholipase C-gamma1, *Biochem Biophys Res Commun 273*, 294-301.
[29] Henderson, M. C., Gonzales, I. M., Arora, S., Choudhary, A., Trent, J. M., Von Hoff, D. D., Mousses, S., and Azorsa, D. O. (2011) High-throughput RNAi screening identifies a role for TNK1 in growth and survival of pancreatic cancer cells, *Mol Cancer Res 9*, 724-732.
[30] Zhu, Y. X., Tiedemann, R., Shi, C. X., Yin, H., Schmidt, J. E., Bruins, L. A., Keats, J. J., Braggio, E., Sereduk, C., Mousses, S., and Stewart, A. K. (2011) RNAi screen of the druggable genome identifies modulators of proteasome inhibitor sensitivity in myeloma including CDK5, *Blood 117*, 3847-3857.

[31] Lierman, E., Van Miegroet, H., Beullens, E., and Cools, J. (2009) Identification of protein tyrosine kinases with oncogenic potential using a retroviral insertion mutagenesis screen, *Haematologica 94*, 1440-1444.
[32] Gu, T. L., Cherry, J., Tucker, M., Wu, J., Reeves, C., and Polakiewicz, R. D. (2010) Identification of activated Tnk1 kinase in Hodgkin's lymphoma, *Leukemia 24*, 861-865.
[33] Hoare, S., Hoare, K., Reinhard, M. K., Lee, Y. J., Oh, S. P., and May, W. S., Jr. (2008) Tnk1/Kos1 knockout mice develop spontaneous tumors, *Cancer Res 68*, 8723-8732.
[34] Ooi, E. L., Chan, S. T., Cho, N. E., Wilkins, C., Woodward, J., Li, M., Kikkawa, U., Tellinghuisen, T., Gale, M., Jr., and Saito, T. (2014) Novel antiviral host factor, TNK1, regulates IFN signaling through serine phosphorylation of STAT1, *Proc Natl Acad Sci U S A 111*, 1909-1914.
[35] Hoare, K., Hoare, S., Smith, O. M., Kalmaz, G., Small, D., and Stratford May, W. (2003) Kos1, a nonreceptor tyrosine kinase that suppresses Ras signaling, *Oncogene 22*, 3562-3577.
[36] May, W. S., Hoare, K., Hoare, S., Reinhard, M. K., Lee, Y. J., and Oh, S. P. (2010) Tnk1/Kos1: a novel tumor suppressor, *Trans Am Clin Climatol Assoc 121*, 281-292; discussion 292-283.
[37] Fennell, L. M., Rahighi, S., and Ikeda, F. (2018) Linear ubiquitin chain-binding domains, *FEBS J 285*, 2746-2761.
[38] Randles, L., and Walters, K. J. (2012) Ubiquitin and its binding domains, *Front Biosci (Landmark Ed) 17*, 2140-2157.
[39] Raasi, S., Varadan, R., Fushman, D., and Pickart, C. M. (2005) Diverse polyubiquitin interaction properties of ubiquitin-associated domains, *Nat Struct Mol Biol 12*, 708-714.
[40] Radley, E. H., Long, J., Gough, K. C., and Layfield, R. (2019) The 'dark matter' of ubiquitin-mediated processes: opportunities and challenges in the identification of ubiquitin-binding domains, *Biochem Soc Trans 47*, 1949-1962.
[41] Jaleel, M., Villa, F., Deak, M., Toth, R., Prescott, A. R., Van Aalten, D. M., and Alessi, D. R. (2006) The ubiquitin-associated domain of AMPK-related kinases regulates conformation and LKB1-mediated phosphorylation and activation, *Biochem J 394*, 545-555.
[42] Murphy, J. M., Korzhnev, D. M., Ceccarelli, D. F., Briant, D. J., Zarrine-Afsar, A., Sicheri, F., Kay, L. E., and Pawson, T. (2007) Conformational instability of the MARK3 UBA domain compromises ubiquitin recognition and promotes interaction with the adjacent kinase domain, *Proc Natl Acad Sci U S A 104*, 14336-14341.
[43] Wang, Y. L., Wang, J., Chen, X., Wang, Z. X., and Wu, J. W. (2018) Crystal structure of the kinase and UBA domains of SNRK reveals a distinct UBA binding mode in the AMPK family, *Biochem Biophys Res Commun 495*, 1-6.
[44] Wu, J. X., Cheng, Y. S., Wang, J., Chen, L., Ding, M., and Wu, J. W. (2015) Structural insight into the mechanism of synergistic autoinhibition of SAD kinases, *Nat Commun 6*, 8953.
[45] Chua, B. T., Lim, S. J., Tham, S. C., Poh, W. J., and Ullrich, A. (2010) Somatic mutation in the ACK1 ubiquitin association domain enhances oncogenic signaling through EGFR regulation in renal cancer derived cells, *Mol Oncol 4*, 323-334.
[46] Pennington, K. L., Chan, T. Y., Torres, M. P., and Andersen, J. L. (2018) The dynamic and stress-adaptive signaling hub of 14-3-3: emerging mechanisms of regulation and context-dependent protein-protein interactions, *Oncogene 37*, 5587-5604.
[47] Mortenson, J. B., Heppler, L. N., Banks, C. J., Weerasekara, V. K., Whited, M. D., Piccolo, S. R., Johnson, W. E., Thompson, J. W., and Andersen, J. L. (2015) Histone deacetylase 6 (HDAC6) promotes the pro-survival activity of 14-3-3zeta via deacetylation of lysines within the 14-3-3zeta binding pocket, *J Biol Chem 290*, 12487-12496.
[48] Johnson, C., Crowther, S., Stafford, M. J., Campbell, D. G., Toth, R., and MacKintosh, C. (2010) Bioinformatic and experimental survey of 14-3-3-binding sites, *Biochem J 427*, 69-78.
[49] Masters, S. C., Yang, H., Datta, S. R., Greenberg, M. E., and Fu, H. (2001) 14-3-3 inhibits Bad-induced cell death through interaction with serine-136, *Mol Pharmacol 60*, 1325-1331.
[50] Dobson, M., Ramakrishnan, G., Ma, S., Kaplun, L., Balan, V., Fridman, R., and Tzivion, G. (2011) Bimodal regulation of FoxO3 by AKT and 14-3-3, *Biochim Biophys Acta 1813*, 1453-1464.

[51] Zheng, Q., Yin, G., Yan, C., Cavet, M., and Berk, B. C. (2004) 14-3-3beta binds to big mitogen-activated protein kinase 1 (BMK1/ERK5) and regulates BMK1 function, *J Biol Chem 279*, 8787-8791.
[52] Yang, H. Y., Wen, Y. Y., Chen, C. H., Lozano, G., and Lee, M. H. (2003) 14-3-3 sigma positively regulates p53 and suppresses tumor growth, *Mol Cell Biol 23*, 7096-7107.
[53] Cheng, L., Pan, C. X., Zhang, J. T., Zhang, S., Kinch, M. S., Li, L., Baldridge, L. A., Wade, C., Hu, Z., Koch, M. O., Ulbright, T. M., and Eble, J. N. (2004) Loss of 14-3-3sigma in prostate cancer and its precursors, *Clin Cancer Res 10*, 3064-3068.
[54] Gasco, M., Bell, A. K., Heath, V., Sullivan, A., Smith, P., Hiller, L., Yulug, I., Numico, G., Merlano, M., Farrell, P. J., Tavassoli, M., Gusterson, B., and Crook, T. (2002) Epigenetic inactivation of 14-3-3 sigma in oral carcinoma: association with p16(INK4a) silencing and human papillomavirus negativity, *Cancer Res 62*, 2072-2076.
[55] Iwata, N., Yamamoto, H., Sasaki, S., Itoh, F., Suzuki, H., Kikuchi, T., Kaneto, H., Iku, S., Ozeki, I., Karino, Y., Satoh, T., Toyota, J., Satoh, M., Endo, T., and Imai, K. (2000) Frequent hypermethylation of CpG islands and loss of expression of the 14-3-3 sigma gene in human hepatocellular carcinoma, *Oncogene 19*, 5298-5302.
[56] Vercoutter-Edouart, A. S., Lemoine, J., Le Bourhis, X., Louis, H., Boilly, B., Nurcombe, V., Revillion, F., Peyrat, J. P., and Hondermarck, H. (2001) Proteomic analysis reveals that 14-3-3sigma is down-regulated in human breast cancer cells, *Cancer Res 61*, 76-80.
[57] Li, D. J., Deng, G., Xiao, Z. Q., Yao, H. X., Li, C., Peng, F., Li, M. Y., Zhang, P. F., Chen, Y. H., and Chen, Z. C. (2009) Identificating 14-3-3 sigma as a lymph node metastasis-related protein in human lung squamous carcinoma, *Cancer Lett 279*, 65-73.
[58] Neupane, D., and Korc, M. (2008) 14-3-3sigma Modulates pancreatic cancer cell survival and invasiveness, *Clin Cancer Res 14*, 7614-7623.
[59] Neal, C. L., Yao, J., Yang, W., Zhou, X., Nguyen, N. T., Lu, J., Danes, C. G., Guo, H., Lan, K. H., Ensor, J., Hittelman, W., Hung, M. C., and Yu, D. (2009) 14-3-3zeta overexpression defines high risk for breast cancer recurrence and promotes cancer cell survival, *Cancer Res 69*, 3425-3432.
[60] Neal, C. L., and Yu, D. (2010) 14-3-3zeta as a prognostic marker and therapeutic target for cancer, *Expert Opin Ther Targets 14*, 1343-1354.
[61] Xu, J., Acharya, S., Sahin, O., Zhang, Q., Saito, Y., Yao, J., Wang, H., Li, P., Zhang, L., Lowery, F. J., Kuo, W. L., Xiao, Y., Ensor, J., Sahin, A. A., Zhang, X. H., Hung, M. C., Zhang, J. D., and Yu, D. (2015) 14-3-3zeta turns TGF-beta's function from tumor suppressor to metastasis promoter in breast cancer by contextual changes of Smad partners from p53 to Gli2, *Cancer Cell 27*, 177-192.
[62] Lu, J., Guo, H., Treekitkarnmongkol, W., Li, P., Zhang, J., Shi, B., Ling, C., Zhou, X., Chen, T., Chiao, P. J., Feng, X., Seewaldt, V. L., Muller, W. J., Sahin, A., Hung, M. C., and Yu, D. (2009) 14-3-3zeta Cooperates with ErbB2 to promote ductal carcinoma in situ progression to invasive breast cancer by inducing epithelial-mesenchymal transition, *Cancer Cell 16*, 195-207.
[63] Kondo, Y., Ognjenovic, J., Banerjee, S., Karandur, D., Merk, A., Kulhanek, K., Wong, K., Roose, J. P., Subramaniam, S., and Kuriyan, J. (2019) Cryo-EM structure of a dimeric B-Raf:14-3-3 complex reveals asymmetry in the active sites of B-Raf kinases, *Science 366*, 109-115.
[64] Park, E., Rawson, S., Li, K., Kim, B. W., Ficarro, S. B., Pino, G. G., Sharif, H., Marto, J. A., Jeon, H., and Eck, M. J. (2019) Architecture of autoinhibited and active BRAF-MEK1-14-3-3 complexes, *Nature 575*, 545-550.
[65] Siveen, K. S., Prabhu, K. S., Achkar, I. W., Kuttikrishnan, S., Shyam, S., Khan, A. Q., Merhi, M., Dermime, S., and Uddin, S. (2018) Role of Non Receptor Tyrosine Kinases in Hematological Malignances and its Targeting by Natural Products, *Mol Cancer 17*, 31.
[66] Agarwal, A., and Tyner, J. W. (2016) RNAi Screening of Leukemia Cells Using Electroporation, *Methods Mol Biol 1470*, 85-94.
[67] Tyner, J. W., Walters, D. K., Willis, S. G., Luttropp, M., Oost, J., Loriaux, M., Erickson, H., Corbin, A. S., O'Hare, T., Heinrich, M. C., Deininger, M. W., and Druker, B. J. (2008) RNAi screening of

the tyrosine kinome identifies therapeutic targets in acute myeloid leukemia, *Blood 111*, 2238-2245.
[68] Bustos, D. M., and Iglesias, A. A. (2006) Intrinsic disorder is a key characteristic in partners that bind 14-3-3 proteins, *Proteins 63*, 35-42.
[69] Sluchanko, N. N., and Bustos, D. M. (2019) Intrinsic disorder associated with 14-3-3 proteins and their partners, *Prog Mol Biol Transl Sci 166*, 19-61.
[70] Uhart, M., and Bustos, D. M. (2014) Protein intrinsic disorder and network connectivity. The case of 14-3-3 proteins, *Front Genet 5*, 10.
[71] Lizcano, J. M., Goransson, O., Toth, R., Deak, M., Morrice, N. A., Boudeau, J., Hawley, S. A., Udd, L., Makela, T. P., Hardie, D. G., and Alessi, D. R. (2004) LKB1 is a master kinase that activates 13 kinases of the AMPK subfamily, including MARK/PAR-1, *EMBO J 23*, 833-843.
[72] Nishimura, I., Yang, Y., and Lu, B. (2004) PAR-1 kinase plays an initiator role in a temporally ordered phosphorylation process that confers tau toxicity in Drosophila, *Cell 116*, 671-682.
[73] Drewes, G., Trinczek, B., Illenberger, S., Biernat, J., Schmitt-Ulms, G., Meyer, H. E., Mandelkow, E. M., and Mandelkow, E. (1995) Microtubule-associated protein/microtubule affinity-regulating kinase (p110mark). A novel protein kinase that regulates tau-microtubule interactions and dynamic instability by phosphorylation at the Alzheimer-specific site serine 262, *J Biol Chem 270*, 7679-7688.
[74] Lennerz, J. K., Hurov, J. B., White, L. S., Lewandowski, K. T., Prior, J. L., Planer, G. J., Gereau, R. W. t., Piwnica-Worms, D., Schmidt, R. E., and Piwnica-Worms, H. (2010) Loss of Par-1a/MARK3/C-TAK1 kinase leads to reduced adiposity, resistance to hepatic steatosis, and defective gluconeogenesis, *Mol Cell Biol 30*, 5043-5056.
[75] Goodwin, J. M., Svensson, R. U., Lou, H. J., Winslow, M. M., Turk, B. E., and Shaw, R. J. (2014) An AMPK-independent signaling pathway downstream of the LKB1 tumor suppressor controls Snail1 and metastatic potential, *Mol Cell 55*, 436-450.
[76] Izaki, T., Kamakura, S., Kohjima, M., and Sumimoto, H. (2005) Phosphorylation-dependent binding of 14-3-3 to Par3beta, a human Par3-related cell polarity protein, *Biochem Biophys Res Commun 329*, 211-218.
[77] Komander, D., Reyes-Turcu, F., Licchesi, J. D., Odenwaelder, P., Wilkinson, K. D., and Barford, D. (2009) Molecular discrimination of structurally equivalent Lys 63-linked and linear polyubiquitin chains, *EMBO Rep 10*, 466-473.
[78] Husnjak, K., and Dikic, I. (2012) Ubiquitin-binding proteins: decoders of ubiquitin-mediated cellular functions, *Annu Rev Biochem 81*, 291-322.
[79] Mueller, T. D., and Feigon, J. (2002) Solution structures of UBA domains reveal a conserved hydrophobic surface for protein-protein interactions, *J Mol Biol 319*, 1243-1255.
[80] Wilkinson, C. R., Seeger, M., Hartmann-Petersen, R., Stone, M., Wallace, M., Semple, C., and Gordon, C. (2001) Proteins containing the UBA domain are able to bind to multi-ubiquitin chains, *Nat Cell Biol 3*, 939-943.
[81] Kulathu, Y., Akutsu, M., Bremm, A., Hofmann, K., and Komander, D. (2009) Two-sided ubiquitin binding explains specificity of the TAB2 NZF domain, *Nat Struct Mol Biol 16*, 1328-1330.
[82] Kim, D. E., Chivian, D., and Baker, D. (2004) Protein structure prediction and analysis using the Robetta server, *Nucleic Acids Res 32*, W526-531.
[83] Agromayor, M., Soler, N., Caballe, A., Kueck, T., Freund, S. M., Allen, M. D., Bycroft, M., Perisic, O., Ye, Y., McDonald, B., Scheel, H., Hofmann, K., Neil, S. J., Martin-Serrano, J., and Williams, R. L. (2012) The UBAP1 subunit of ESCRT-I interacts with ubiquitin via a SOUBA domain, *Structure 20*, 414-428.
[84] O'Hare, T., Shakespeare, W. C., Zhu, X., Eide, C. A., Rivera, V. M., Wang, F., Adrian, L. T., Zhou, T., Huang, W. S., Xu, Q., Metcalf, C. A., 3rd, Tyner, J. W., Loriaux, M. M., Corbin, A. S., Wardwell, S., Ning, Y., Keats, J. A., Wang, Y., Sundaramoorthi, R., Thomas, M., Zhou, D., Snodgrass, J., Commodore, L., Sawyer, T. K., Dalgarno, D. C., Deininger, M. W., Druker, B. J., and Clackson, T. (2009) AP24534, a pan-BCR-ABL inhibitor for chronic myeloid leukemia,

potently inhibits the T315I mutant and overcomes mutation-based resistance, *Cancer Cell 16*, 401-412.
[85] Shannon, P., Markiel, A., Ozier, O., Baliga, N. S., Wang, J. T., Ramage, D., Amin, N., Schwikowski, B., and Ideker, T. (2003) Cytoscape: a software environment for integrated models of biomolecular interaction networks, *Genome Res 13*, 2498-2504.
[86] Kim, H. K., Kim, J. W., Zilberstein, A., Margolis, B., Kim, J. G., Schlessinger, J., and Rhee, S. G. (1991) PDGF stimulation of inositol phospholipid hydrolysis requires PLC-gamma 1 phosphorylation on tyrosine residues 783 and 1254, *Cell 65*, 435-441.
[87] Wang, Z., Gluck, S., Zhang, L., and Moran, M. F. (1998) Requirement for phospholipase C-gamma1 enzymatic activity in growth factor-induced mitogenesis, *Mol Cell Biol 18*, 590-597.
[88] Ren, X., Duan, L., He, Q., Zhang, Z., Zhou, Y., Wu, D., Pan, J., Pei, D., and Ding, K. (2010) Identification of Niclosamide as a New Small-Molecule Inhibitor of the STAT3 Signaling Pathway, *ACS Med Chem Lett 1*, 454-459.
[89] Panjarian, S., Iacob, R. E., Chen, S., Engen, J. R., and Smithgall, T. E. (2013) Structure and dynamic regulation of Abl kinases, *J Biol Chem 288*, 5443-5450.
[90] Seet, B. T., Dikic, I., Zhou, M. M., and Pawson, T. (2006) Reading protein modifications with interaction domains, *Nat Rev Mol Cell Biol 7*, 473-483.
[91] Cabe, M., Rademacher, D. J., Karlsson, A. B., Cherukuri, S., and Bakowska, J. C. (2018) PB1 and UBA domains of p62 are essential for aggresome-like induced structure formation, *Biochem Biophys Res Commun 503*, 2306-2311.
[92] Peng, H., Yang, J., Li, G., You, Q., Han, W., Li, T., Gao, D., Xie, X., Lee, B. H., Du, J., Hou, J., Zhang, T., Rao, H., Huang, Y., Li, Q., Zeng, R., Hui, L., Wang, H., Xia, Q., Zhang, X., He, Y., Komatsu, M., Dikic, I., Finley, D., and Hu, R. (2017) Ubiquitylation of p62/sequestosome1 activates its autophagy receptor function and controls selective autophagy upon ubiquitin stress, *Cell Res 27*, 657-674.